Catarina Costa e Marques

Bachelor in Micro and Nanotechnologies Engineering

Application of vanadium oxide nanoparticles in smart surfaces

Dissertation submitted in partial fulfillment
of the requirements for the degree of

Master of Science in
Micro and Nanotechnologies Engineering

Adviser: Rita Maria Mourão Salazar Branquinho, Full Professor, NOVA University of Lisbon

Co-adviser: Alexandra Maria Ferreira Gonçalves, Master, CENIMAT

Examination Committee

Chairperson: Dr. Rodrigo Ferrão de Paiva Martins
Raporteurs: Dr. João Pedro Botelho Veiga
Dr. Rita Maria Mourão Salazar Branquinho

FACULDADE DE CIÊNCIAS E TECNOLOGIA
UNIVERSIDADE NOVA DE LISBOA

September, 2018

Application of vanadium oxide nanoparticles in smart surfaces

This document was created using the (pdf)LaTeX processor, based in the "novathesis" template[1], developed at the Dep. Informática of FCT-NOVA [2].
[1] https://github.com/joaomlourenco/novathesis [2] http://www.di.fct.unl.pt

"Someone is sitting in the shade today because someone planted a tree a long time ago."
Warren Buffett

Acknowledgements

In this segment I would like to recognize all the people who had some kind of influence through this five years and helped to turned me the person I am.

Firstly, I would like to thank my mother and friends, specially, Tiago Gonçalves who was always ready to help and to give moral support, to Jaissica Vassantrai, Catarina Rijo, Miguel Furtado, Rita Fragoso, Manuel Chapa, Débora Magalhães, João Teles and Vanessa Lopes who encourage and support me along this past five years.

To my advisers Rita Branquinho and Alexandra Gonçalves who turn possible to make a master thesis mainly focused in Vanadium oxides and their help along these path.

To the remaining members of the group Luís Pereira, Ana Pimentel, Joana Pinto, Sónia Pereira and Daniela Gomes who supported me along my work, helped to elucidate my doubts and providing me with XRD and SEM analysis. A special thanks to Alexandra Gonçalves for her help in the lab.

To all my mates in BEST Almada, without you life in university would never be the same.

At last, I want to send my gratitude to Dra. Elvira Fortunato and Dr. Rodrigo Martins who allowed me to realize my master thesis in CENIMAT.

Abstract

Vanadium oxides (VO_x) have been extensively investigated due to their many phases and range of properties, such as eletrochromic, thermochromic and electrochemical. Therefore, this promising materials may be implemented as energy efficiency materials in many sectors like military, industrial, domestic and transport.

In the present dissertation VO_x phases and nanostructures have been synthesized by hydrothermal synthesis using microwave irradiation as heating source. The synthesis parameters, such as reducing agent, dissolution method and the hydrothermal parameters temperature, reducing agent concentration and ratios were vary and studied to observe their impact in morpholy and the resultant VO_x phase.

Several pure and combination of VO_x phases were achieved, such as VO_2 (B), V_6O_{13}, V_3O_7, VO_2 (M2) and V_2O_5. The structural composition and morphology of the as-obtained powders were characterized by X-ray diffraction (XRD) and scanning electron microscopy (SEM), respectively. Additionally, to observe a possible transition temperature of the samples a thermogravimetry and differential scanning calorimetry (TG-DSC) analysis were performed.

Furthermore, nanosheets were layered in fluorine doped tin oxide (FTO) and Indium tin oxide (ITO) and applied as cathode, with a maximum current of 1.75 mA for ITO and 1.46 mA for FTO.

Keywords: Vanadium oxides, hydrothermal synthesis, microwave irradiation, nanosheets, phase transitions.

Resumo

Os óxidos de vanádio têm sido extensivamente investigados devido à sua diversidade de fases e variedade de propriedades, tais como eletrocrómicas, termocrómicas e eletroquímicas. Por isso, estes materiais promissores podem ser implementados como materiais energeticamente eficientes em vários setores, nomeadamente, militar, indústria, doméstico e transportes.

Na presente dissertação as fases e estruturas de VO_x foram sintetizadas por método hidrotermal usando como fonte de aquecimento a radição por microondas. Os parâmetros de síntese, tais como agente de redução, método de dissolução e os parâmetros hidrotermais, temperatura, concentração do agente de redução e rácios foram variados e estudados de forma a observar o seu impacto na estrutura morfológica e na fase de VO_x resultante.

Várias combinações de fases VO_x foram alcançadas, nomeadamente VO_2 (B), V_6O_{13}, V_3O_7, VO_2 (M2) e V_2O_5. A composição estrutal e morfológica dos pós obtidos, foram caracterizados por difração de raios-X (DRX) e microscopia eletrónica de varrimento (SEM), respetivamente. Adicionalmente, para observar uma possível transição de fase por aumento de temperatura das amostras, foram realizadas análises de termo-gravimetria e de calorimetria diferencial de varrimento (TG-DSC).

Ademais, nanosheets foram depositadas em fluorine tin oxide (FTO) e indium tin oxide (ITO) e aplicadas como cátodo com uma corrente máxima de 1.75 mA para o ITO e 1.46 mA para o FTO.

Palavras-chave: Óxidos de vanádio, síntese hidrotermal, radiação por microondas, nanosheets, transições de fase.

Contents

List of Figures

List of Tables

ΔT_{sol}	Modulation of solar energy.
Cs	Crystal structure.
EC	Electrochromic.
Sg	Space group.
T_C	Transition temperature.
T_{lum}	Luminous transmittance.

Acronyms

AACVD	Aerosol assisted chemical vapour deposition.
APCVD	Atmosphere pressure chemical vapour deposition.
CVD	Chemical vapour deposition.
FTO	Fluorine doped tin oxide.
ICSD	Inorganic crystall structure database.
ITO	Indium tin oxide.
MIT	Metal-to-insulator.
NIR	Near-infrared radiation.
PLD	Pulsed laser deposition.
PVD	Physical vapour deposition.
SEM	Scanning Electron microscopy.
TG-DSC	Thermogravimetry and differential scanning calorimetry.
UV	Ultra violet.
VO_x	Vanadium oxide phases.
XRD	X-Ray diffractions.

Motivation and objectives

With the fast evolution of technology it is important to explore and optimize strategies to reduce the energy on demand and store it. Industrial, transportation and domestic are worldwide sectors which consume finite primary resources, such as, petroleum, coal and natural gas.

Although there was a rapid response, by using renewable resources, due to the inherent environmental problems associated with fossil fuels, like global warming and climate change, it is vital to reduce energy usage and heat loss in buildings by enhance the energy efficiency of the structures.

Vanadium oxides have been extensively investigated due to their large variety of oxidation states and wide range of promising potential applications in a variety of sectors, since they are still a source of innovative developments.

The aim of this work is to study the influence of several parameters, such as molar ratio, temperature, reducing agent concentrations, dissolution method and reducing agents in the hydrothermal synthesis of vanadium oxide nanoparticles phases and morphologies using hydrothermal synthesis assisted by microwave irradiation and their possible application.

V_6O_{13}, V_3O_7, V_2O_5 and VO_2 (B) nanoparticles were obtained by microwave irradiation in laboratory, analysed and characterized in CENIMAT.

1

Introduction

Nowadays with the increase use of energy due to climate change impact it is imperative to reduce the loss of energy used in buildings and transportation. The need for renewable and intelligent energy control was the start for the research for new materials, their evolution and optimization [1]. In this regard, functional materials and energy efficiency devices, like thermochromic, electrochemical and electrochromic materials have become a subject of research [2].

Vanadium oxides have been widely studied due to their peculiar chemical, physical and electrical properties and promising potential applications such as cathode in lithium-ion batteries [5], infrared sensors [5], thermochromic windows [6], optical devices and adaptive infrared camouflage technology [7]. Vanadium generally presents synthesis difficulties due to its existence in several oxidation states [8].

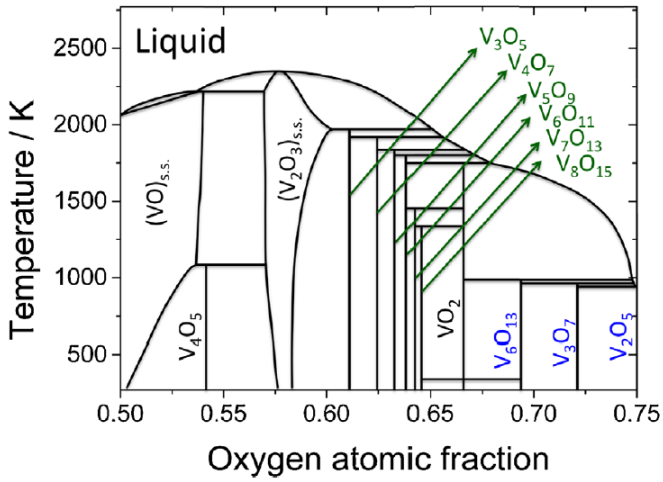

Figure 1.1: Phase diagram of vanadium oxides, where the Magnéli series is highlighted in blue and the Wadsley series is highlighted in green [9].

Their oxidation states (2^+ to 5^+), correspond to a diversity of oxides, including single valence oxides (e.g. VO_2 and V_2O_5) and mixed valence oxides (e.g. V_4O_6 and V_6O_{13}) as shown in table 1.1 [10, 11].

Table 1.1 show different vanadium oxide phases and their correspondent transition temperature, crystalline structure, and space group.

Vanadium oxide phases and corresponding crystalline structure, such as VO_2 (A) tetragonal, VO_2 (M) monoclinic-rutile and VO_2 (R) tetragonal-rutile have thermochromic features and optical switching properties [12], while VO_2 (B) monoclinic, V_6O_{13} monoclinic and V_2O_5 orthorhombic present high electrochemical capacity [16–18].

With their unique colour change, electrochromic materials have a reversible change in their optical characteristics due to external applied voltages allowing industrial applications, in particular smart windows, optical shutters in airplanes sunglasses and reflective displays [3].

Table 1.1: Vanadium oxide compounds and VO_2 polymorphs.

Phase	**T_c [°C]**	**Crystalline structure (CS)**	**Space group (SG)**	**Ref.**
VO_2 (A)	162	Tetragonal	$P4_2/ncm$	[12]
VO_2 (B)	-	Monoclinic	C2/m	[12]
VO_2 (M)	68	Monoclinic-Rutile	$P2_1/c$	[13]
VO_2 (R)	68	Tetragonal-Rutile	$P4_2/mnm$	[12, 13]
V_6O_{13}	-123, -218	Monoclinic	C2/m	[14]
V_2O_5	257	Orthorhombic	Pmmn	[14, 15]

Electrochromic materials are distinguished by properties that are reversible, through the application of electrical current or voltage [19]. This field is quickly expanding in regard to implement windows and glass facades for energy-efficient buildings, since energy efficiency in the buildings has often been forgotten as an opportunity for CO_2 reduction [19].

Electrochromic window devices are capable to control the solar radiation passage by applying a small voltage, their colour and optical properties changes allowing an effective way to regulate the solar transmittance [2, 19, 20]. As a result a change occurs in transmittance of the visible and near infrared spectra depending on the presence and absence of external voltage on the electrochromic layer [2].

This windows are constituted by a substrate, TCO, working electrode (cathode, counter electrode (anode) and an electrolyte as exemplified in figure 1.2.

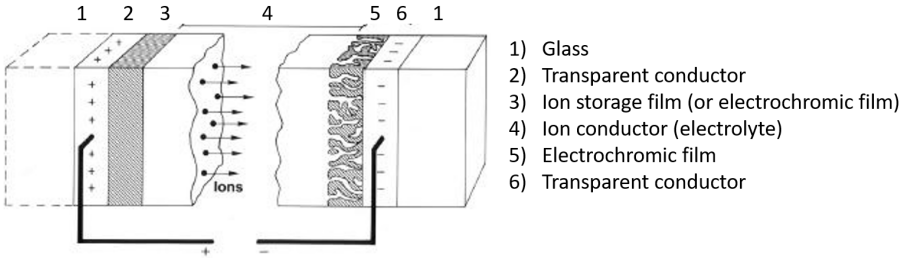

Figure 1.2: Schematic illustration of a generic electrochromic (EC) device design. The arrows illustrate the transport of positive ions in an electrical field [19].

Thermochromic materials, can vary their properties with the variation of temperature in a certain range. This effect can be described as the material ability to modify its reflection properties, in a certain region of the electro-magnetic spectrum, because of temperature variations [4].

Nevertheless, thermochromic vanadium oxides has some performance limitations namely, a temperature transition (T_C) at 68 °C, which is a high value for daily applications, an inadequate modulation of solar energy (ΔT_{sol}) and poor luminous transmittance (T_{lum}).

1.1 Vanadium dioxide (VO_2)

VO_2 is a particularly fascinating system for investigators due to his herculean structural diversity [21]. During the past few years, VO_2 (B) has increased the interest of researchers in the field of energy technologies, because of its layered structure and moderate work potential connected to a high energy capacity [22]. In addition, this polymorph can be transformed into VO_2 (A), (R) and (M) [12, 21, 22].

For the reason explained above, the majority of the studies efforts have been dedicated to the improvement and elaboration of 1D nanostructured VO_2 (B) materials (e.g., nanorods, nanowires, nanoribbons, nanospheres and nanobelts) and their electrochemical performances [22].

Among the numerous crystalline VO_2 phases reported (e.g. VO_2(A), VO_2(B), VO_2(C), VO_2(M), VO_2(R)) [12, 4, 23–25] the monoclinic phase, VO_2 (M), presents a metal-to-insulator (MIT) phase where a reversible structural change occurs from infrared-transparent semiconducting phase (VO_2 (M)), to an infrared-translucent metallic phase (VO_2 (R)), exhibiting a high IR reflectance. In other words, VO_2 (M) is transparent to infrared radiation, below transition temperature (T_C), and reflects part of the near infrared radiation (NIR) above T_C [4, 26, 27]. Only VO_2 (M) has a fully reversible MIT when heated above its T_C [13].

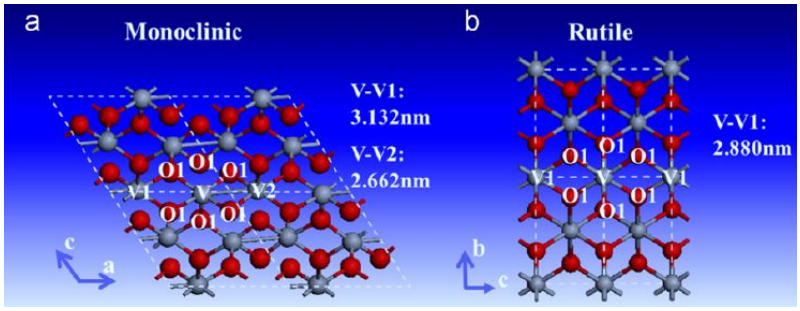

Figure 1.3: Crystalline structures of monoclinic VO2 (M) (a) and rutile type VO2 (R) (b). The gray and red balls denote V and O atmos in the cells,respectively. The titled zig-zag like V atmos (marked with V1–V–V2 in(a)) become equidistant (V atoms marked with V1–V–V1 in(b)) after the metal-insulator phase transition [26].

The change in the optical properties makes VO_2 (M) a potential candidate for applications in buildings materials, since it presents an automatic response to an environmental temperature change without the use of a switching device [4, 27, 28].

Smart windows, Fig. 1.4, for example are an excellent application of this polymorph for daily use. Despite that, T_C must be lowered near to room temperature (25-30^{o}C), in order to decrease the energy usage [29]. In this regard by doping VO_2 (M) T_C can be minimized with high valence cations, such as Nb^{5+}, Mo^{6+}, Ta^{5+} and W^{6+} and adjust the solar modulation and transmittance [29, 30]. To increase T_C low valence cations, like Ti^{2+} and Ga^{3+}, are used. [29].

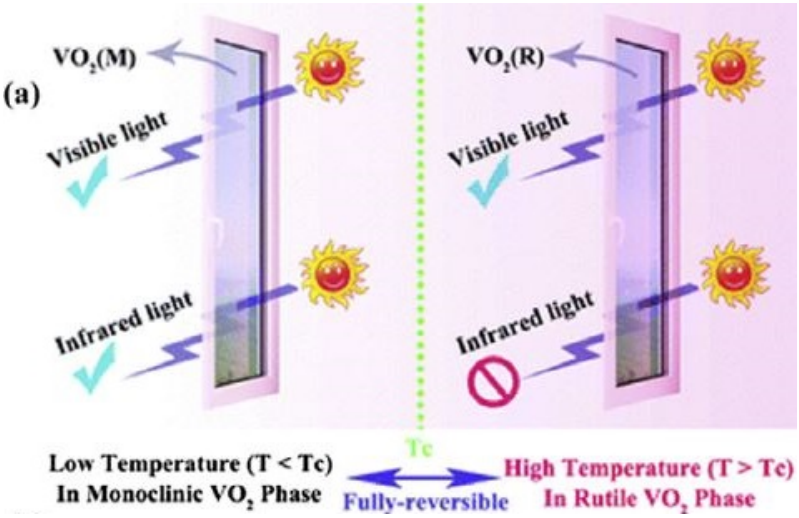

Figure 1.4: Example of a thermochromic window with vanadium dioxide [2].

Also, the modulation of solar energy ΔT_{sol} (integral transmittance between 240 nm and 2600 nm) is insufficient and luminous transmittance T_{lum} (integral transmittance between 380 nm and 780 nm) is low [29, 31]. To increase these values to the desirable T_{lum}>40% and ΔT_{sol}>10%,there are many approaches including the addition of an anti-reflection coatings and doping [32, 33].

Many methods were reported in literature to produce VO_2 (M), such as gas-based deposition like physical vapour deposition (PVD) [34], atmosphere pressure chemical vapour deposition (APCVD) [34], aerosol assisted chemical vapour deposition (AACVD)[14, 29] among others, however, these techniques imply high costs, complex equipment and require vacuum or reduced pressure conditions [14].

Solution based synthesis, such as hydrothermal or solvothermal method and sol-gel synthesis [35, 36], are a large scale and low cost way of production, uses low temperature and allows to adjust the parameters during the reaction [16, 4, 37].

1.2 Hexavanadium tridecaoxide (V_6O_{13})

Currently, with the increase of portable electronic consumer devices, electric vehicles, and large-scale electricity storage in smart or intelligent grids, the search for rechargeable batteries that can repeatedly generate clean electricity from stored materials and convert reversely electric energy into chemical energy with efficient electrochemical reliable energy storage and conversion has increased [38, 39]. In addition, adopting ways to minimise energy utilization and energy conservation is an important demand to decrease the amount of CO_2 originated from energy production [19].

V_6O_{13} is a mixed-valence compound belonging to the Magnéli phase (V_nO_{2n-1}) as an intermediate between VO_2 (V^{4+}) and V_2O_5 (V^{5+}) [16, 40, 41]. At high temperatures has a paramagnetic metallic behaviour, while at low temperatures has a semiconductor-to-metal

transition T_C at -123ºC and an antiferromagnetic transition at -218ºC [40, 41].

Among the vanadium oxides, V_6O_{13} is a potential candidate as a battery cathode material for Li-ion batteries (LIB) and as a supercapacitor due to its electrochemical properties [16, 42] and fully reversible insertion/discharge (lithiation) process. V_6O_{13} passes through a succession of phase transitions, and hosts as many as six Li atoms per V_6O_{13} unit [14], as shown in figure 1.5.

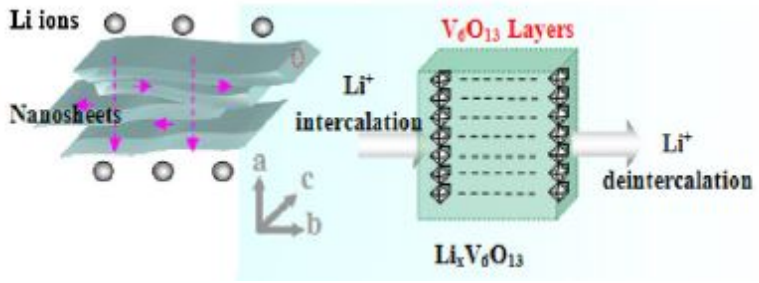

Figure 1.5: Schematic illustration of the movement of lithium in $Li_xV_6O_{13}$ [10].

The operating properties of a battery depend not only on the structure, but also on the morphology of the electrode components [22, 42]. Many morphologies have been reported such as, nanosheets [5, 10], belt-like particles [43], micro-flowers [38], nano-architectures [16], hollow-flowers [42] among others.

Although there are no conclusions in which morphology is better, nanosheets offer a good electrolyte ion storage spaces and faster transport path for electrolyte ions and electrons, guiding the improvement of electrochemical behaviours [44].This structure turns possible the contact between the cathode material and electrolyte, inducing a more active absorption and abruption of Li ions in the cathode material [10].

The synthesis of stoichiometric V_6O_{13} is difficult because of the possible lattice defect in the metastable V_6O_{13}, which might involve a stacking disorder during the oxidation/reduction [10]. Several methods to synthesise V_6O_{13} have been reported either physical or chemical.

By physical deposition there are CVD [45] and PLD [46], between others, however, physical methods are expensive and their experimental conditions are energy consuming [43]. Nonetheless, the most used are hydrothermal and solvothermal routes [16, 43] since it is more advantageous due to low cost manufacturing and ultra-low power consumption.

Many hydrothermal synthesis have been reported by S. Xu [5], Y. Zang [43], H. Fei [38], G. Mutta [16], Z. Huang [42], N. Peys [11], Z. Zou [10], among others.

In this work microwave irradiation is prefered as heat source over conventional oven due to its many advantages, such as a faster reaction in reduced time because of the internal heating on the vessel is developed by the friction and collision between molecules, control of certain parameters which in conventional heating is not possible and energy saving [4, 47].

2

Materials and methods

2.1 Materials

Vanadium pentoxide (V_2O_5, from Sigma-Aldrich, assay > 98 %), oxalic acid dihydrate ($C_2H_2O_4.2H_2O$, from Merck, assay > 99.5%), citric acid ($C_6H_8O_7$, from Sigma-Aldrich, assay > 99.5 %), Tungsten trioxide (WO_3, from Sigma-Aldrich, assay > 99.9 %), deionized water (H_2O), ethanol (C_2H_6O) and isopropyl alcohol (C_3H_8O).

2.2 Hydrothermal synthesis of VO_x

Two procedures were performed, the first with oxalic acid and the second with citric acid [48] as reducing agents. Vanadium pentoxide was fixed at 0.5 g, 25 g/L of vanadium pentoxide concentration, and all powders were used without further purification.

Vanadium pentoxide and oxalic acid dihydrate, 1:(1-4) (V_2O_5:oxalic acid) molar ratio respectively, were dissolved in 20 mL of deionized water by sonication or magnetic stirring from 30 minutes to 2 hours. At this stage the solution, initially yellow, turns to green indicating that V^{5+} was not completely reduced to V^{4+}.

Hydrothermal synthesis was carried out by microwave irradiation where the parameters temperature and pressure were kept in the range of [140, 180] (°C) and [150, 250] (Psi), respectively and time was held constant at 20 minutes. After cooling, in the microwave, the resultant black powder was filtered from the supernatant blue solution and centrifugated with deionized water, ethanol or isopropyl alcohol for several times. Finally, the as-prepared powder was dried by a vacuum process at 65 °C for 12 hours.

The prepared samples were then annealed in a furnace in high purity nitrogen atmosphere, to prevent oxidation, and cooled down until room temperature. The chemical reaction of vanadium oxide formation from vanadium pentoxide can be represented by equation 2.1.

$$V_2O_5 + C_2H_2O_4 \cdot 2H_2O \longrightarrow 2VO_2 + 2CO_2 + 3H_2O \tag{2.1}$$

The second procedure was conducted with citric acid (Sigma-Aldrich, 99,5%) and vanadium pentoxide (Sigma-Aldrich 98%), 1:(1-3) (V_2O_5:citric acid) molar ratio respectively. The powders were dissolved in 20 mL of deionized water by stirring for 1h and 30 minutes. As written above, the yellow solution turns into green implicating that V^{5+} was not completely reduced to V^{4+}.

The hydrothermal synthesis was lead and the product also cooled in the microwave, as represented by the chemical equation 2.2. The deposited powder was filtered from the supernatant blue solution and centrifugated with isopropyl alcohol for a few minutes, a number of times. At last, the prepared powders were dried by a vacuum process at 65 °C for 12 hours.

The resultant powder was then annealed in a furnace in high purity nitrogen, as well, to prevent oxidation.

$$V_2O_5 + C_6H_2O_4 + 3\,O_2 \longrightarrow 2\,VO_2 + 6\,CO_2 + H_2O \tag{2.2}$$

Also, in order to dope the resultant powders a small amount of tungsten trioxide was added to the solutions prepared using 26 and 50 g/L of citric acid and to the 50 and 67 g/L of oxalic acid before the dissolution occurred. The following steps remained the same as written above.

2.3 Characterization Methods

Morphological characterization of the synthesized powders was performed by scanning electron microscopy (SEM-FIB Carl Zeiss AURIGA CrossBeam) with an Oxford X-ray energy dispersive spectroscopy (EDS) which allows detection of chemical elemental composition of the sample.

To analyse the phase of the VO_x samples X-Ray diffraction (XRD) was performed using a PANalytical X'Pert PRO MPD X-ray diffractometer, equipped with an X'Celerator 1D detector and using CuKα radiation. The XRD data were acquired in the Bragg-Brentano configuration and the samples were scanned from 10° to 90° 2θ with a step size of 0.033° 2θ and accumulating a time of 33 s per 2θ position.For phase identification the XRD patterns of the samples were compared to standard patterns from the Inorganic Crystal Structure Database (ICSD).

In order to observe the transition temperatures thermal analysis was conducted by thermogravimetry and differential scanning calorimetry (Simultaneous Thermal Analyser (TGA-DSC–STA 449 F3 Jupiter)), where 25 mg of as-prepared powders were loaded into an open Pt/Rh crucible.

Two analysis were performed, the first under inert atmosphere starting at room temperature for annealing and the second under a oxidizing atmosphere with a heating rate of 10 K/min from room temperature until 260 °C to observe a possible phase transition temperature.

A UV-vis-NIR Spectroscopy PerkinELmer Lambda 950 analysis with temperature was performed with a Harrick's Praying Mantis reflection accessory equipped with a reaction chamber from 250 nm to 2500 nm, which permits to observe the optical reflectance behaviour of the sample. The temperature of the powders was controlled using Harrick's automatic temperature controller. IR emission measurements of the powedrs were complemented by using an IR camera (DIAS infrared system – PYROVIEW 380L / 50Hz / 30° x 23° compact). Due to a lamp change at 800 nm noise is observed in the graphics.

3

Results and discussion

3.1 VO_x synthesis using citric acid as reducing agent

3.1.1 Influence of process parameters on VO_x morphology

In this section the procedure of the synthesis was kept constant, namely stirring for ninety minutes, temperature at 180 °C, pressure at 250 Psi, power at 250 W, while stirring; citric acid concentration; 26 g/L and 50 g/L concentrations and washing process were varied to assess if these parameters would influence VO_x morphology. The following SEM images show the powders washed with isopropyl alcohol.

SEM images (Fig. 3.1), reveal that the stirring method has an important role in morphology. First, it is important to note that the prevailing structure in VO_2 nanoparticles is nanoplatelets regardless of the concentration used (26 g/L or 50 g/L citric acid).

Althought the samples with concentration of 26 g/L, 1:1 (V_2O_5:citric acid) molar ratio, show a homogeneous structure in each phase, magnetic stirring originates rounded agglomerates, while with sonication there is aggregation of nanoplatelets. The nanoplatelets structure is originated by the liquid-exfoliation derived from the sonication, as reported in literature [49].

In contrast, each sample with 50 g/L of citric acid concentration 1:2 (V_2O_5:citric acid) molar ratio, appears with two phases, loose nanoplatelets and rounded agglomerates as it is possible to observe in Fig. 3.1 b.

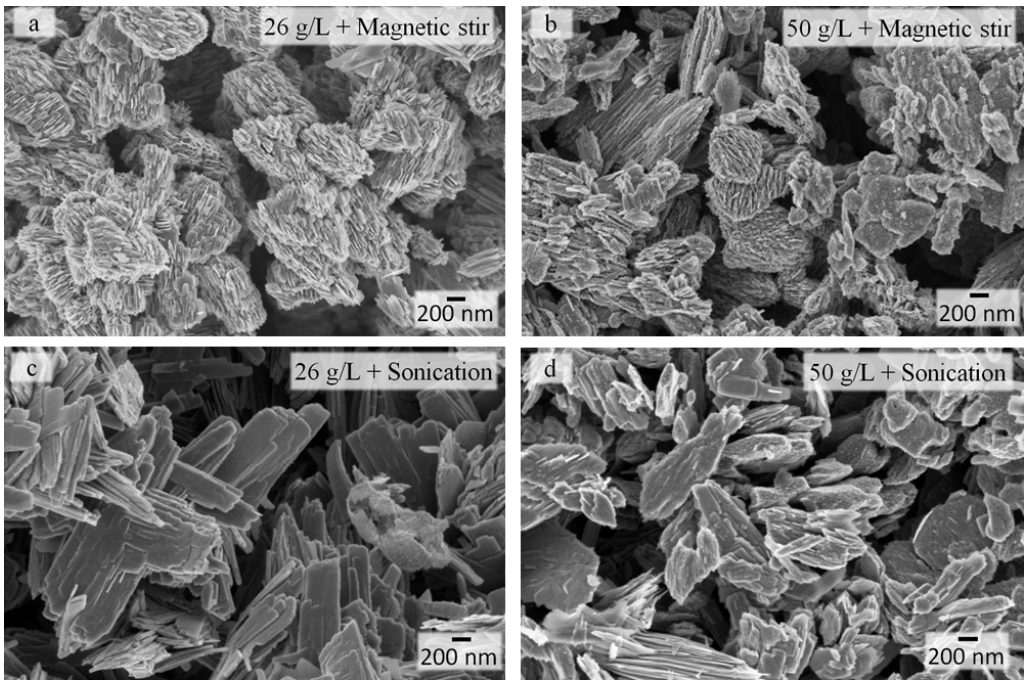

Figure 3.1: Morphology difference between a) and b) magnetic stirring and c) and d) sonication.

The resultant powders prepared using 50 g/L of citric acid as reducing agent, with 1:2 (V_2O_5:citric acid) molar ratio, magnetic stirring for one hour and thirty minutes at 180 °C were then washed with either deionized water (Fig. 3.2 a)) or ethanol (Fig. 3.2 b)).

From the direct analysis of the SEM images (Fig. 3.2), since they present an aggregated spherical shape in both SEM images the cleanse of the resultant powders with deionized water or ethanol has no impact in the nanostructures.

However, by comparing with the sample of 50 g/L concentration, 1:2 (V_2O_5:citric acid) molar ratio, washed with isopropyl alcohol, Fig. 3.1 b), the nanostructures are completely different, except for the aggregation of the particles present in the three samples.

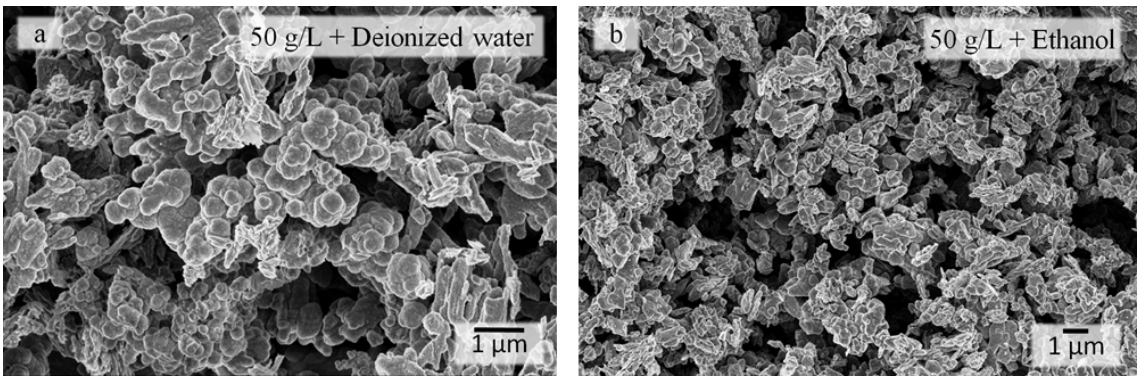

Figure 3.2: Washing the resultant powders with a) deionized water and b) ethanol.

3.1.2 Influence of the synthesis parameters

3.1.2.1 Reagent concentration and ratios

Concentrations and reagent ratios play an important role in the achievement of VO_x phases, since to the synthesis process initiate $V(5^+)$ must be reduced to $V(4^+)$.

The experimental molar ratio ranged from 1:(1-4)(V_2O_5:citric acid), however, only 1:(1-2) molar ratio, corresponding to 26 g/L and 50 g/L of citric acid concentrations, had a resulting black powder in a blue solution, while ratios from 1:(3-4) had just a supernatant blue solution and no VO_x powders were obtained, as stated in Table 3.1. Further experiments were carried out, namely the annealing of the powders, in an inert atmosphere, to see if a phase change occurred, the results can be observed in Table 3.2.

XRD analysis of the annealed samples were carried out to determine the VO_x phases for each annealing temperature. The results of the XRD diffractograms are represented in Fig. 3.3.

Table 3.1: Summary of molar ratios, citric acid concentrations and resultant powders.

(V_2O_5:citric acid) molar ratio	Citric acid concentration (g/L)	Resultant powders
1:1	26	VO_2 (B)
1:2	50	VO_2 (B)
1:3	79	-
1:4	105	-

Table 3.2: Results of the as-prepared powders at different annealing temperatures.

	Temperature (°C)			
Citric acid concentration (g/L)	300	350	400	450
26	VO_2 (B)	VO_2 (B)	V_2O_5 + V_6O_{13}	V_3O_7 + V_6O_{13} + V_2O_5
50	VO_2 (B)	V_3O_7		VO_2 (B) + VO_2 (M2)

Fig. 3.3 a), shows the diffraction patterns of the 26 g/L sample. The main peaks may be indexed to VO_2 (B) (ICSD #01-081-2392), space group C2/m, lattice parameters a=12.0930 Å, b=3.7021 Å and c=6.4330 Å, with the main planes (110), (001) and (002). With the temperature increasing until 350 °C the peaks remained mostly unchanged, leading one to believe that there is no structural change in the sample.

Starting at 400 °C a possible combination of phases is observed, between monoclinic V_6O_{13} (ICSD #01-075-1140), space group C2/m, lattice parameters a=11.9220 Å, b=3.6800 Å and c=10.1380 Å, with the main peaks (110), (003) and (200) and orthorhombic V_2O_5 (ICSD #98-002-2114), space group P m m n, lattice parameters a=3.5640 Å, b=11.5120 Å, c=4.3680 Å, with the main orientation planes (001), (110) and (040).

At 450 °C new peaks appear and a new combination of phases is seen. The peaks (-111), (600) and (204) may appear from a monoclinic V_3O_7 phase (ICSD #01-071-0454), space group C2/c, lattice parameters a=21.9210Å, b=3.6790Å and c=18.3410Å.

For the samples with 50 g/L, Fig. 3.3 b), each temperature reveals a different phase. At the temperature of 300 °C the main indexed peaks are presumed to VO_2 (B) (ICSD #01-081-2392), with the same peaks described before. While at the 350 °C a monoclinic V_3O_7 phase (ICSD #01-071-0454) may be the pure phase represented, since the indexed peaks in the diffraction samples correspond to the relative intensity of the pattern.

Also, a possible presence at 450 °C of monoclinic VO_2 (M2) (ICSD #98-005-6236), space group C2/m, lattice parameters a=9.0830 Å, b=5.7630 Å and c=4.5320Å, (201), with 2θ values of 36.9° correlated with (220) and (20-1) planes, 27.7° with (20-1) and (201) planes, and 55.3° with (421) orientation plane, respectively. A plane overlaid of the first

two 2θ values is likely, since the peaks are broad. In addition, monoclinic VO_2 (B) (ICSD #01-081-2392) may be indexed to several peaks of the same diffraction pattern.

Firstly, based in the investigated results, it is possible to conclude that different concentrations lead to different phases, since a thermochromic phase is observed at 50 g/L of citric acid concentration, whereas V_2O_5 orthorhombic phase appears at 26 g/L of citric acid concentration, leading to the belief that concentration is a critical factor in the VO_x synthesis.

However, as the XRD diffractograms show, increasing temperature boosts the probability of a phase combinations occurring, because in both concentrations at 450 °C a combination of two or more phases is achieved. This may happen because during the annealing time, the pressure of nitrogen may not have been enough to have a fully converted phase. Lattice parameters were taken from the correspondent diffraction pattern.

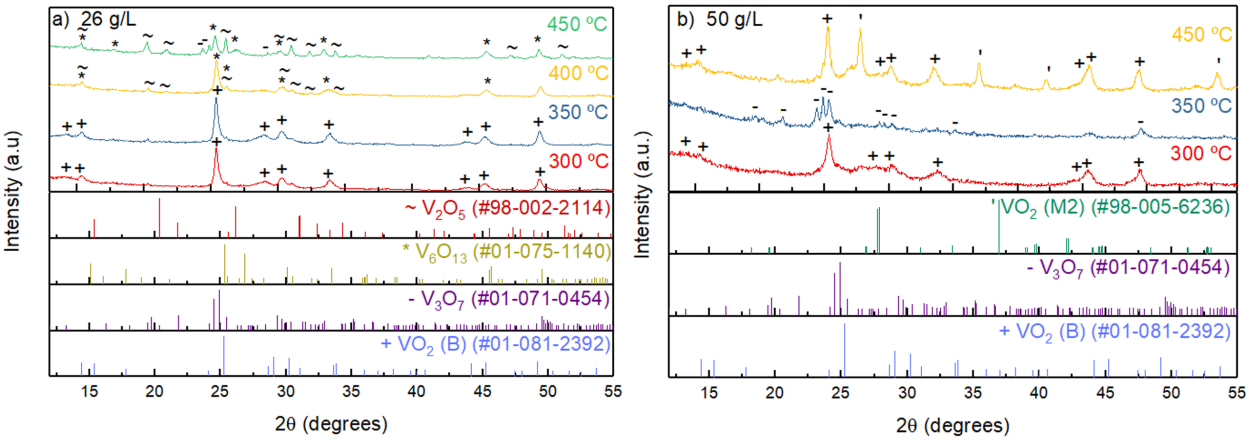

Figure 3.3: XRD diffractograms of samples with a) 26 g/L and b) 50 g/L citric acid concentrations at different annealing temperatures.

After the XRD analysis a DSC thermogram of the 50 g/L annealed at 450 °C was conducted to investigate if a possible phase transition was present. The VO_x powder obtained with 50 g/L of citric acid concentration and annealed at 450 °C were analysed under an oxygen atmosphere from room temperature to 260 °C.

In Fig. 3.4 the DSC thermogram shows a small broad endothermic peak at 81 °C and at 155 °C for the 50 g/L of citric acid concentration sample. To confirm the results the analysis was runned twice and the outcome remained similar.

Usually, the monoclinic thermochromic phase of VO_2 appears with a transition temperature of 68 °C for the transition metal-insulator (MIT) [13, 4], however the current results do not fit in the thermochromic behaviour.

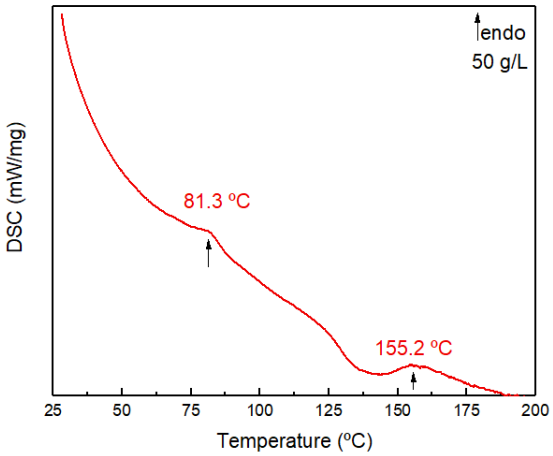

Figure 3.4: DSC thermogram, in air, of the 50 g/L of citric acid concentration annealed powder at 450 °C.

3.1.2.2 Synthesis temperature

The study of hydrothermal synthesis temperature impact was carried out by varying the temperature from 140 °C to 190 °C and by keeping the remaining parameters constant, namely 50 g/L of citric acid concentration, 1:2 (V_2O_5:citric acid) molar ratio, magnetic stirring for ninety minutes, pressure at 250 Psi, 250 W of power and the resultant powders washed with isopropyl alcohol. Fig. 3.5 reveals how the crystalline structure is influenced by synthesis temperature. A likely pure phase of VO_2 (B) (ICSD #01-081-2392) was obtained at 160 °C, 170 °C and 180 °C , since the main peaks (110), (001) and (002) were indexed.

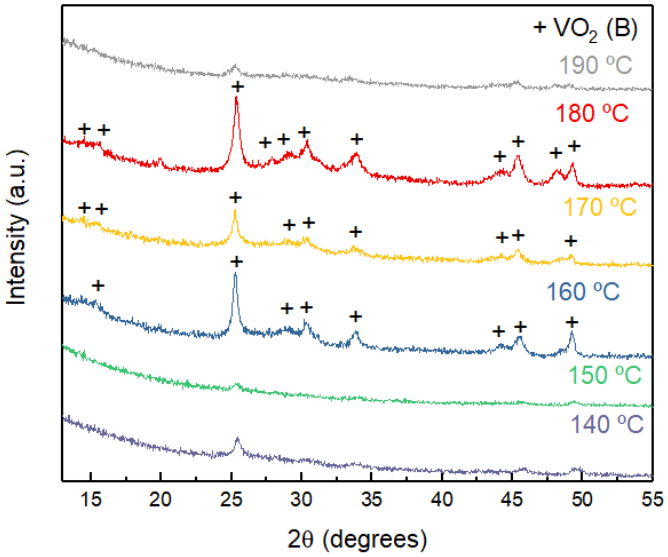

Figure 3.5: XRD diffraction patterns of the resultant powders of 50 g/L of citric acid concentration samples synthesized at different temperatures.

As can be seen in Fig. 3.5, at 140 °C, 150 °C and 190 °C the samples did not show a

good crystalline structure to index peaks to a specific phase with confidence.

According to literature the formation of VO_2 (B) by hydrothermal synthesis assisted by microwave irradiation starts at 160 °C [4]. The results in Fig. 3.5 are consistent with literature, since temperatures below 160 °C and above 190 °C do not lead to a good crystalline structure.

Taking everything into consideration, due to a combination of high temperatures (160, 170 and 180 °C) and pressure (250 Psi) from the hydrothermal synthesis assisted by microwave irradiation a good crystalline structure of a VO_2 (B) phase is reached.

3.1.3 Influence of doping with WO_3 on VO_x properties

Doping with different oxides can be used to change the properties of VO_x, in specific its transition temperature. WO_3 is the most common dopant used in VO_2 due to its high valence cations which replace vanadium atoms in its crystal structure [4].

The procedure of the doped powders start with the dissolution of citric acid, concentration of 26 g/L, 1:1(V_2O_5:citric acid) molar ratio and 50 g/L, 1:2(V_2O_5:citric acid) molar ratio, vanadium pentoxide and 0.0310 g (3 wt% and 2 wt% of WO_3, respectively) of WO_3 in deionized water under magnetic stirring for ninety minutes. Then, a hydrothermal treatment, at 180 °C, was carried out. After the cooling, the as-prepared powders were washed three or more times with isopropyl alcohol.

XRD analyses were carried out as shown in Fig.3.6 to confirm the presence of WO_3 and VO_x, respectively. The diffractograms note (002), (020), (200) and (202) main peaks corresponding to monoclinic tungsten oxide, space group $P2_1/n$ (ICSD #00-043-1035), for both concentrations and orthorhombic V_2O_5 (ICSD #98-002-2114), space group P m m n, with the main peaks (001), (110) and (040) for 26 g/L. For the 50 g/l concentration no VO_x phase was possible to index.

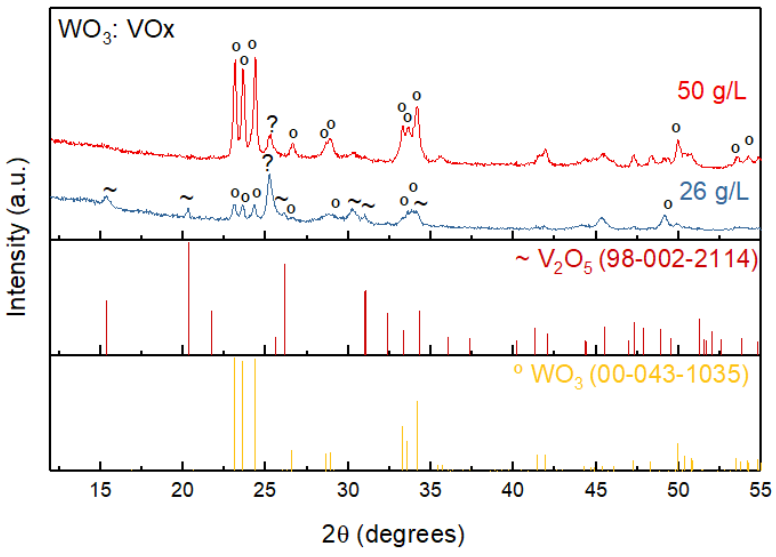

Figure 3.6: XRD diffractograms of as-prepared doped VO_x powders with the diffraction patterns corresponding to V_2O_5 and WO_3.

It is interesting to note that 26 g/L of citric acid sample have intense VO_x peaks, while in 50 g/L of citric acid sample, WO_3 peaks are more intense. In addition, after annealed the doped powders crystalline structure remained unaltered.

These results lead to the conclusion that a combination of VO_x and WO_3 phases was achieved since it is possible to identify the separated phases, not knowing if the W atoms are diffused in the crystalline structure of VO_x.

SEM images were taken before and after annealing, Fig. 3.7, to observe if doping would have an impact in the morphological structure of the samples. As first impression a morphological difference is perceived, since at the sample prepared using 26 g/L of citric acid only loose and agglomerate nanoplatelets are observed, while at 50 g/L of citric acid concentration rounded spherical shape structures are surrounding the nanoplatelets, as shown in Fig. 3.7 b) and d), respectively.

Also, the spherical shape structures do not appear in the 26 g/L sample, which can be attributed to the beginning of WO_3 diffusion in the crystalline structure of VO_x. Since the concentration of WO_3 used was the same in both concentrations (26 g/L and 50 g/L of citric acid) the structural difference may be due to the reaction kinetics, leading to the belief that a lower concentration of reducing agent benefit the diffusion of W atoms into the crystalline structure of VO_x.

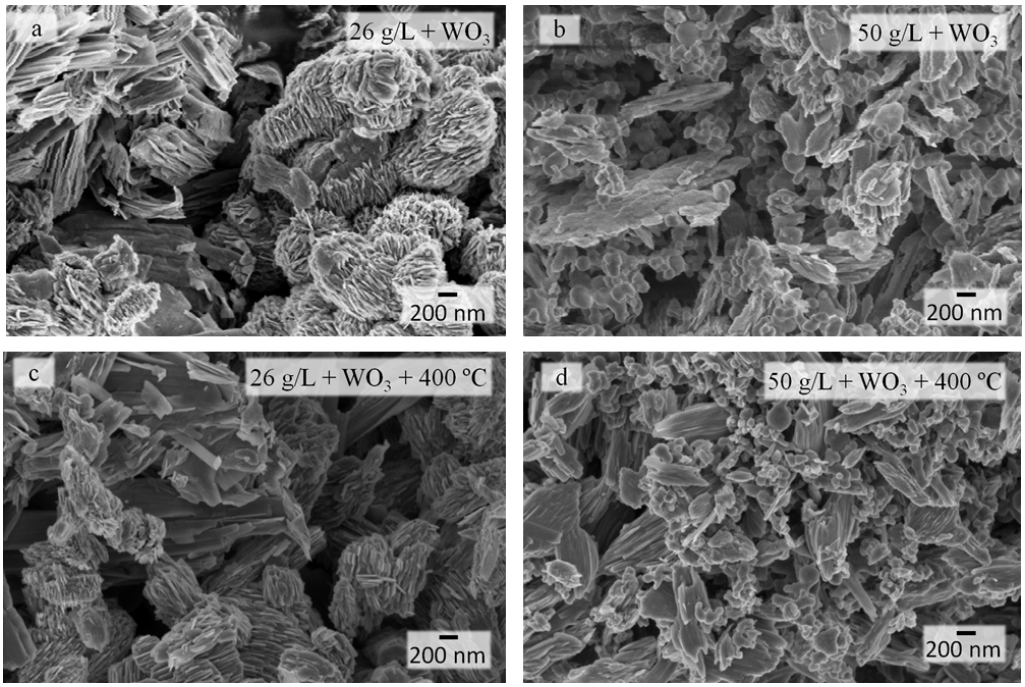

Figure 3.7: SEM images of the doped powders a) and b) before and c) and d) after annealing.

3.2 VO_x synthesis using oxalic acid as reducing agent

3.2.1 Influence of process parameters on VO_x morphology

Similarly to what was performed when using citric acid as reducing agent, SEM images were taken to perceive if the different oxalic acid concentrations (67, 50, 35, 25 and 18 g/L), washing and dissolution method impact morphology.

The 50 g/L of oxalic acid concentration, 1:3 (V_2O_5:oxalic acid) molar ratio, and 35 g/L of oxalic acid concentration, 1:2 (V_2O_5:oxalic acid) molar ratio, samples were synthesized under the same hydrothermal parameters, temperature at 180 °C, a dissolution of two hours and washed with deionized water.

The effect of stirring on morphology of the resultant material is clearly evident when using 50 g/L oxalic acid concentration (Fig. 3.8) since the sonicated powders have nanosheets and the magnetic stirred powders nanoplatelets, while, the not stirred sample does not present a specific morphology. The presence of nanosheets in Fig. 3.8 a) can be explained due to the liquid-exfoliation lead by sonication, as reported in literature [49].

For the resultant powders of 35 g/L oxalic acid concentration, Fig. 3.9, similar morphologies are shown. Nanoplatelets are in both concentrations, nevertheless, in the magnetic stirred samples the particles are thinner than the sonicated samples, leading to believe that sonication and magnetic stirring did not significantly influenced the morphology, in this specific concentration.

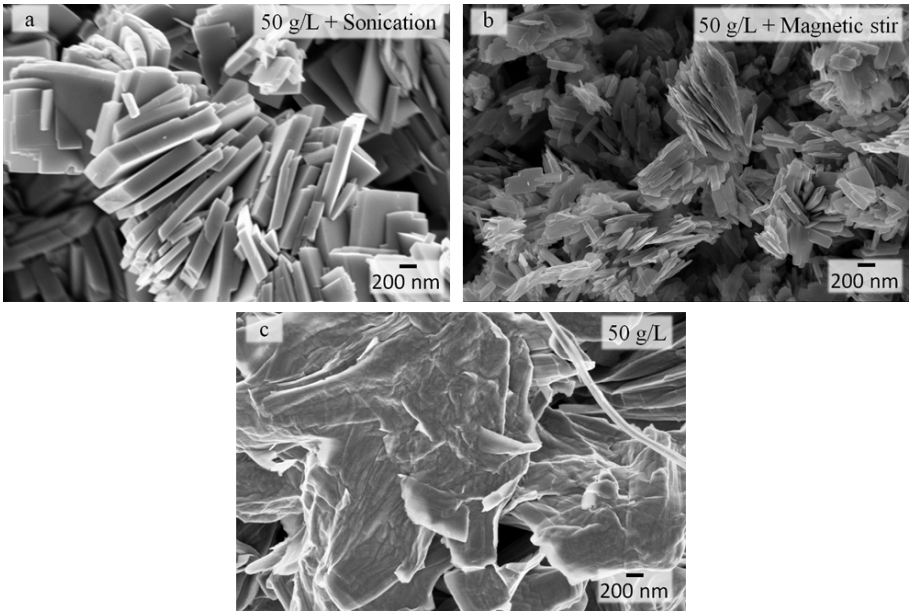

Figure 3.8: SEM images of the as-prepared powders prepared with oxalic acid concentration of 50 g/L, using a) sonication, b) magnetic stirring and c) non-stirred.

By comparing the nanoplatelets structure, the 35 g/L oxalic acid concentration appears with a square shape, whereas the 50 g/L oxalic acid concentration has a rectangular shape,

leading to the conclusion that concentration influence the morphology and the dissolution method at higher concentrations.

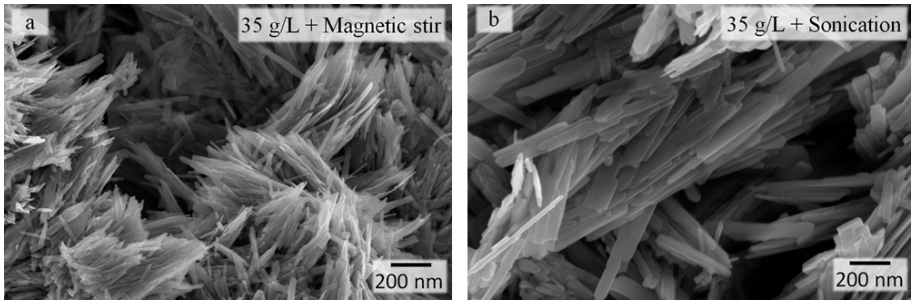

Figure 3.9: Direct comparison of dissolution methods, a) magnetic stirring and b) sonication, of 35 g/L oxalic acid concentration.

For the observation of the oxalic acid concentration influence, the resultant powders of samples prepared with 18, 25, 35, 50 and 67 g/L oxalic acid concentration were dissolved under magnetic stirring for one hour and thirty minutes, synthesized under the same hydrothermal parameters, temperature at 180 °C, and washed with isopropyl alcohol.

In Fig. 3.10 it is possible to observe that by increasing the concentration the morphology evolves from a non specific structure, to aggregated nanoplatelets to well structured nanosheets.

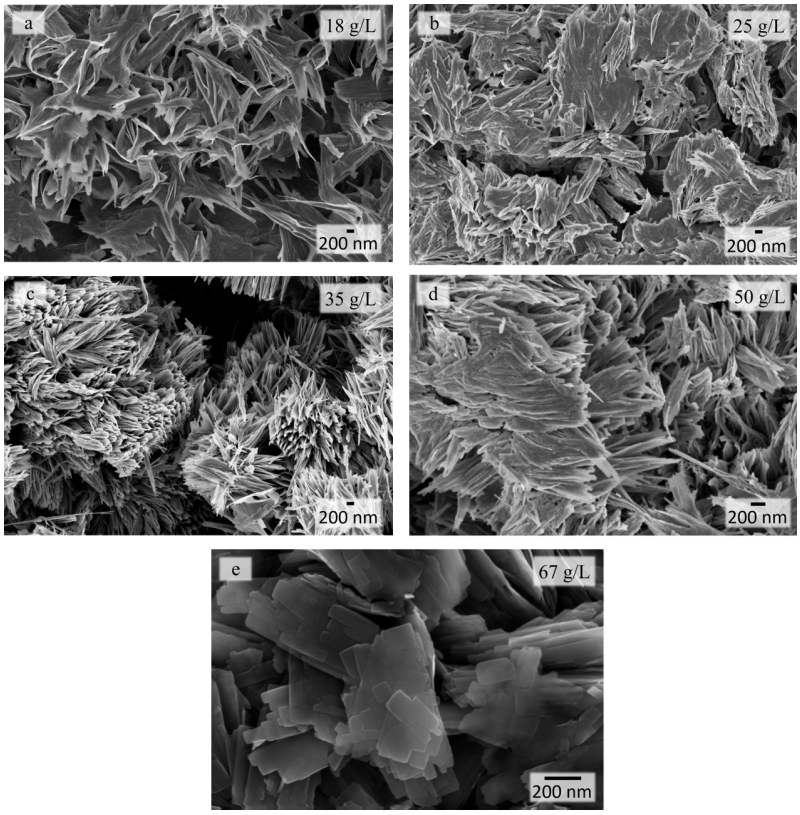

Figure 3.10: SEM images of a) 18 g/L, b) 25 g/L, c) 35 g/L, d) 50 g/L and e) 67 g/L oxalic acid concentrations.

The direct analysis of the SEM images allows the deduction that oxalic acid concentration has an important role in morphology of the resultant powders. Also, low concentrations of oxalic acid, namely 25 and 35 g/L, induces nanoplatelets agglomeration, whereas high concentrations, namely 50 and 67 g/L of oxalic acid, creates nanosheets, as already observed previously.

The influence of the washing step was determined for the resultant product of 25 g/L oxalic acid concentration. A molar ratio of 1:1.44 was dissolved with magnetic stirring for ninety minutes, a 160 °C temperature for hydrothermal synthesis and washed with ethanol, Fig. 3.11 a) and with ispropyl alcohol Fig. 3.11 b).

The SEM images below reveal the same morphological structure, nanoplatelets, however with different shapes for each powder. The one washed with ethanol shows a loose square shape nanoplatelet, while with isopropyl alcohol an aggregated rectangular shape nanoplatelet is observed. Being nanoplatelets the basic structure, it is possible to infer that washing only influences the structures shape.

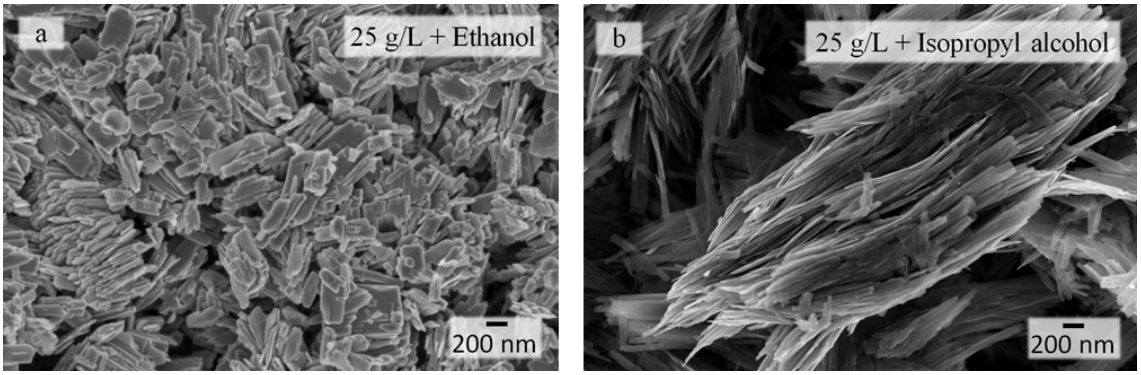

Figure 3.11: SEM images of the as-prepared powders washed with a) ethanol and b) isopropyl alcohol.

3.2.2 Influence of the synthesis parameters

3.2.2.1 Reagents concentration and ratio

As reported in literature [13, 50] reagents ratios and concentration have an important role in order to fully reduce vanadium (5^+) to (4^+) and obtain VO_2. Molar ratio ranged from 1:(1-4) (V_2O_5:oxalic acid), however, samples synthesized with molar ratios higher than 1:3 did not achieved a resultant powder, as Table 3.3 shows.

All samples were synthesized under the same hydrothermal parameters, temperature at 180 °C, dissolved under sonication for two hours and washed with deionized water.

Table 3.3: Oxalic acid concentrations and molar ratios.

Molar ratio	Concentration (g/L)	Resultant powder
1:1	18	V_2O_5
1:1.44	25	VO_2 (B)
1:2	35	VO_2 (B)
1:2.08	38	-
1:1.51	44	-
1:3	50	VO_2 (B)
1:3	67	VO_2 (B)
1:1.51	75	-
1:2.78	100	-

From Table 3.3, samples with 35 and 50 g/L, 1:2 and 1:3 (V_2O_5:oxalic acid) molar ratios respectively, were chosen to be annealed at different temperatures under inert atmosphere. In Table 3.4 XRD results of the annealed powder are summarised. In Fig. 3.12 the XRD diffraction patterns can be seen.

The diffractograms of the samples prepared with oxalic acid concentration of 35 g/L before annealing shows, VO_2 (B) monoclinic space group C2/m (ICSD #01-081-2392), lattice parameters a=12.0930 Å, b=3.7021 Å and c=6.4330 Å, with the main directions (001), (110) and (002). While at 350 °C and 550 °C the present phase is V_2O_5 orthorhombic, space group P m m n (ICSD #98-002-2114), lattice parameters a=3.5640 Å, b=11.5120 Å and c=4.3680 Å, where the (001), (110) and (040) main directions are present.

The XRD diffractograms corresponding to the sample prepared with 50 g/L of oxalic acid concentration suggests the phase VO_2 (B) monoclinic (ICSD #01-081-2392) before annealing and at 350 °C, with the main planes (001), (110) and (002) and V_6O_{13} phase (ICSD #01-075-1140) emerge at 300 °C with the main peaks (110), (003) and (-401).

It has been reported in literature that the following phases can be originated in the order $VO_2 \rightarrow V_6O_{13} \rightarrow V_2O_5$ [8] and $V_6O_{13} \rightarrow VO_2 \rightarrow V_2O_5$ [16], because V_6O_{13} is an oxidation state between $V(5^+)$ and $V(4^+)$, while in VO_2 (B) only $V(4^+)$ is present.

From this direct analysis it is possible to conclude that the concentration of the reducing agent, in this case oxalic acid, has indeed an influence in the production of a certain VO_x phase, after annealing. Samples with lower concentration resulted in VO_2 (B) and V_2O_5, which also appear in the lower concentration (26 g/L of citric acid) of Fig. 3.3 a), while with the higher concentration of oxalic acid the thermochromic phase was not observed.

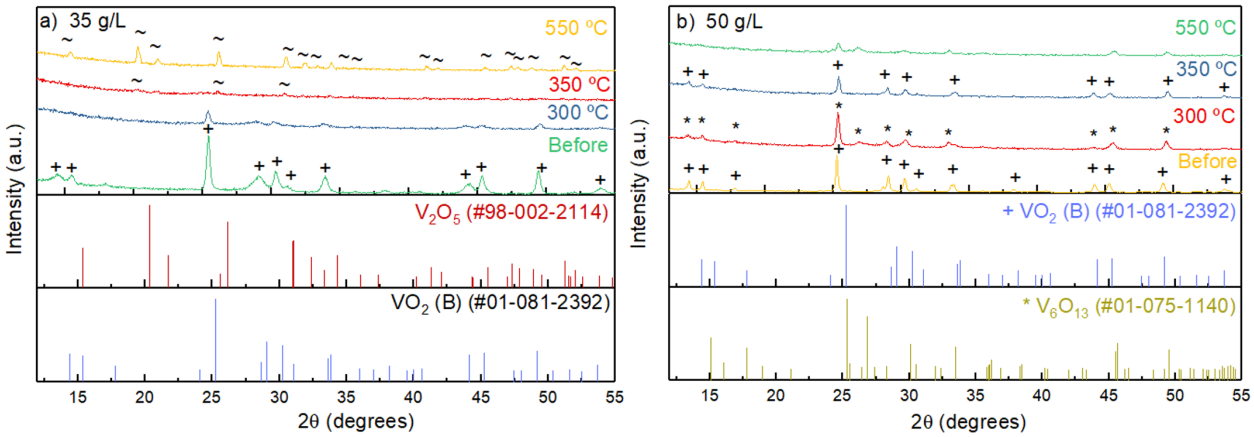

Figure 3.12: XRD diffractograms patterns of the annealed as-prepared VO_2 (B) powders with a) 35 g/L and b) 50 g/L of oxalic acid concentrations.

Table 3.4: Annealing temperature results of the samples prepared using 35 g/L and 50 g/L of oxalic acid concentration.

	Temperature (°C)			
Oxalic acid concentration (g/L)	Before annealing	300	350	550
35	VO_2 (B)		V_2O_5	V_2O_5
50	VO_2 (B)	V_6O_{13}	VO_2 (B)	

For the sample prepared using 50 g/L of oxalic acid concentration, 1:3 (V_2O_5:oxalic acid) molar ratio, a DSC thermogram analysis and a UV-vis-NIR reflectance spectroscopy test of the annealed powder at 550 °C were performed. The DSC thermogram was carried out from room temperature to 200 °C under oxidizing atmosphere, and shows a very broad peak at 119.5 °C, Fig.3.13 b). So, further DSC analysis under the same conditions were carried out to see if the very broad peak was maintained, and the new results continue with the same value. Also, all powders prepared with 35 g/L, 67 g/L and 25 g/L of oxalic acid show a value in a range between 114 °C to 119 °C in their DSC thermogram.

After the DSC thermogram, to observe if the as-prepared powder had an optical change, a UV-vis-NIR reflectance spectroscopy analysis was performed to the same annealed powder. The sample was first analysed at room temperature and then in a 20 °C interval. In Fig. 3.13 a), an overall 2% difference in reflectance was obtained between 25 °C and 180 °C, besides, this value is sufficient to conclude that the annealed powder does not show a thermochromic behaviour.

With further interpretation of all results, the powders corresponding to the VO_2 (B) and V_6O_{13}, do not present a thermochromic behaviour.

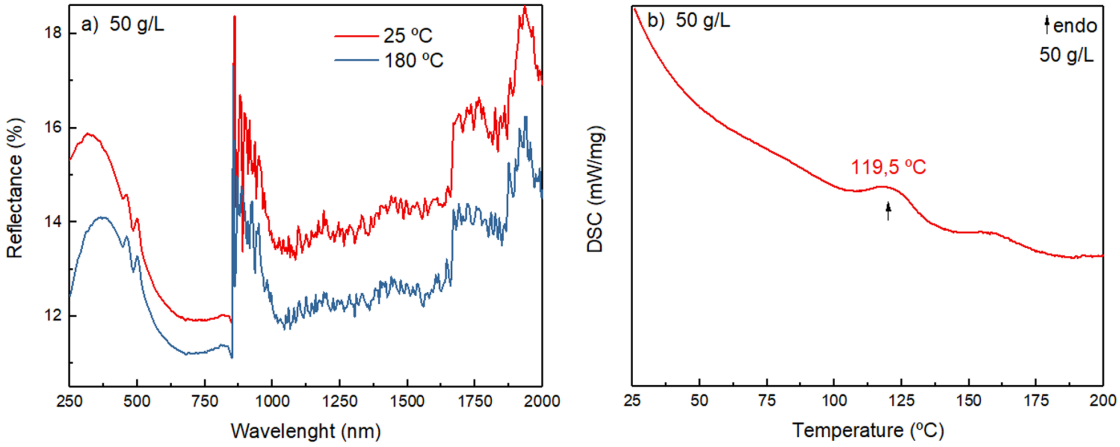

Figure 3.13: Analysis of a) reflectance pattern of the annealed as-prepared sample prepared using 50 g/L of oxalic acid concentration powders and b) DSC thermogram.

3.2.2.2 Synthesis temperature

The analysis of the temperature influence during the hydrothermal synthesis was carried out by varying the temperatures from 140 °C to 200 °C while keeping constant the remaining variables, namely a sample prepared with 50 g/L 1:3 (V_2O_5:oxalic acid) concentration, two hours of sonication, pressure at 250 Psi, power at 250 W, twenty minutes of hydrothermal synthesis and washing with deionized water.

XRD diffraction patterns represented in Fig. 3.14 demonstrate samples prepared using 50 g/L of oxalic acid concentration on a range of temperatures from 140 °C to 180 °C. At 190 °C the result was a supernatant blue solution and the temperature of 200 °C was never reached during the hydrothermal synthesis due to the limitation of the equipment.

With the temperature increase, the crystallinity of the samples increases and different VO_x phases appear. At 140 °C the current phase peaks may be attributed to V_2O_5 orthorombic (ICSD #98-002-2114), while at 150 °C no diffraction peaks could be properly identified.

From 160 °C a probable pure monoclinic phase of V_6O_{13} (ICSD #01-075-1140), with the main planes (110), (003) and (220) is observed, while at 170 °C and 180 °C the orientation main planes (110), (001) and (002) may be attributed to the monoclinic VO_2 (B) phase (ICSD #01-081-2392).

High temperatures are beneficial for the formation of higher degree crystallization of VO_2 (B) at 180 °C, however, temperatures over 190 °C inhibits the synthesis of powder.

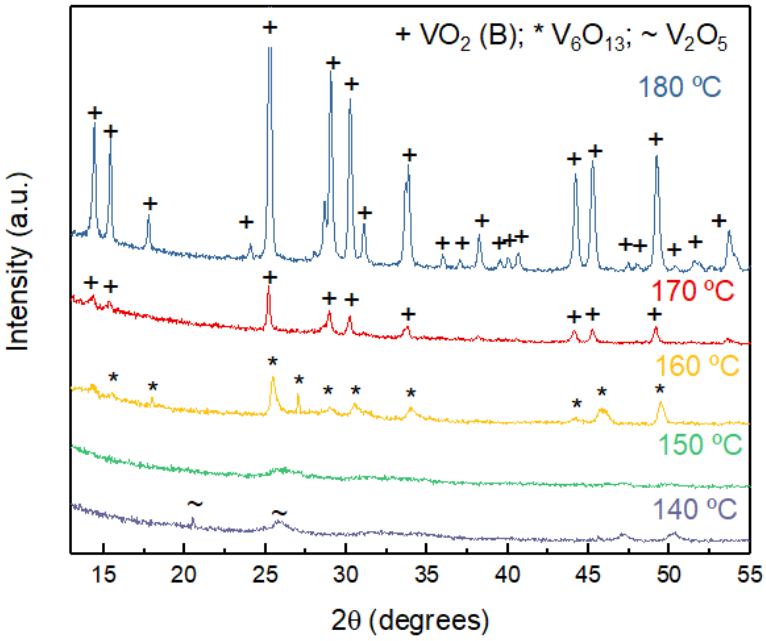

Figure 3.14: XRD diffraction patterns of samples prepared using 50 g/L of oxalic acid concentration at different synthesis temperatures.

3.2.3 Influence of doping with WO_3 on VO_x properties

WO_3 was also used as dopant for the oxalic acid, as explained for the synthesis using citric acid as reducing agent.

The prepared samples had a 50 g/L and 67 g/L of oxalic acid concentration as reducing agent. In order to have the maximum of dissolution of the dopant, 0.015 g (1 wt% of WO_3)of WO_3 was added to the solutions and magnetic stirred for sixty minutes and sonicated for thirty minutes. Afterwards, the solutions were synthesized at 180 °C by microwave irradiation and washed several times with deionized water and ethanol.

The as-obtained doped powders where first studied by XRD analysis, and results are presented in Fig. 3.15. The detected peaks can be assigned to the monoclinic phase VO_2 (B) (ICSD # 01-081-2392), main peaks at (110), (111) and (002). In addition, the presence of WO_3 (ICSD #00-043-1035) is possible to confirm by the main peaks (002), (020) and (200). Considering both phases were present in the XRD analysis, it can be inferred that a combination of phases, instead of doping, was achieved, since WO_3 did not diffused in the crystalline structure of VO_2 (B).

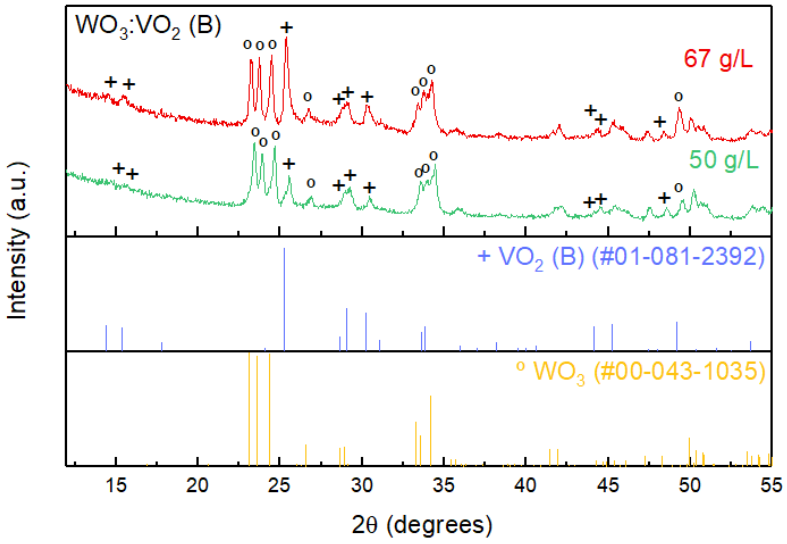

Figure 3.15: XRD diffractograms of as-prepared 50 g/L and 67 g/L of oxalic acid concentration doped with WO_3 and the VO_2 (B) and WO_3 diffraction patterns.

To observe the behaviour of the as-prepared phase combination, a DSC thermogram was executed on the annealed powder at 550 °C for the sample prepared using 50 g/L of oxalic acid concentration. Fig. 3.16 shows a very broad endothermic peak at 121.2 °C and to confirm if the value remained the same, further DSC analyses were performed, under the same circumstances, and the value continued to be 121 °C.

The sample was analysed at room temperature and measured in 20 °C intervals. The results from UV-vis-NIR reflectance spectroscopy analysis does not show any change in reflectance, confirming the sample does not have a thermochromic behaviour.

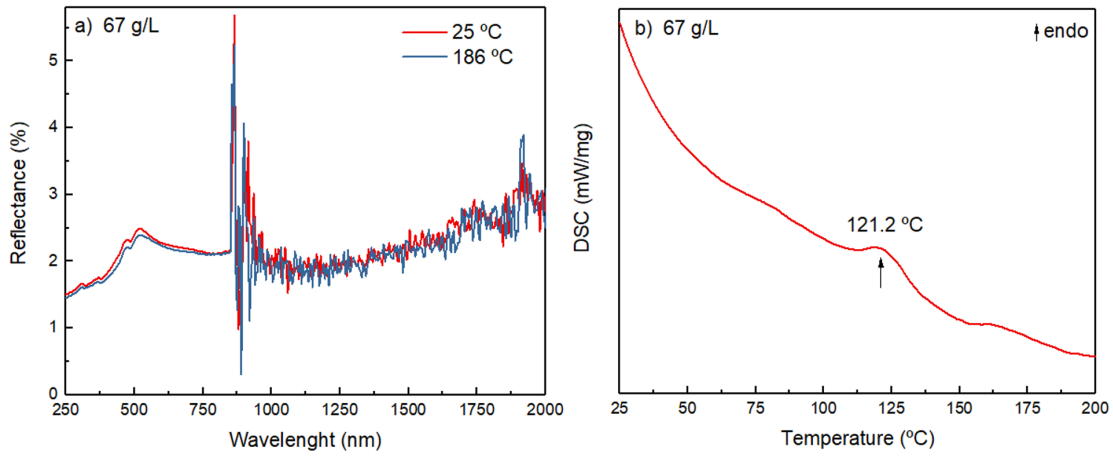

Figure 3.16: Analysis of a) a UV-vis-NIR reflectance spectroscopy and b) a DSC thermogram of as-prepared doped powder prepared using a concentration of 67 g/L oxalic acid.

Fig. 3.17 shows SEM images of the samples prepared using 50 g/L and 67 g/L of oxalic acid concentration. From this images, the basic structure are rectangular shape nanoplatelets covered with nanospheres. By comparing the present SEM images with

Fig. 3.7 b), the morphological structures nanoplatelets likely belong to VO_2 (B), while nanospheres to WO_3.

This images reveal that the combination of WO_3 and VO_2 (B) phases has impact on the nanostructure morphology, although the 67 g/L sample appear to have thinner nanoplatelets than the 50 g/L, the main structure continues to be nanoplatelets, now surrounded by nanospheres. The main differences may be due to the oxalic acid concentration influence on the synthesis of WO_3.

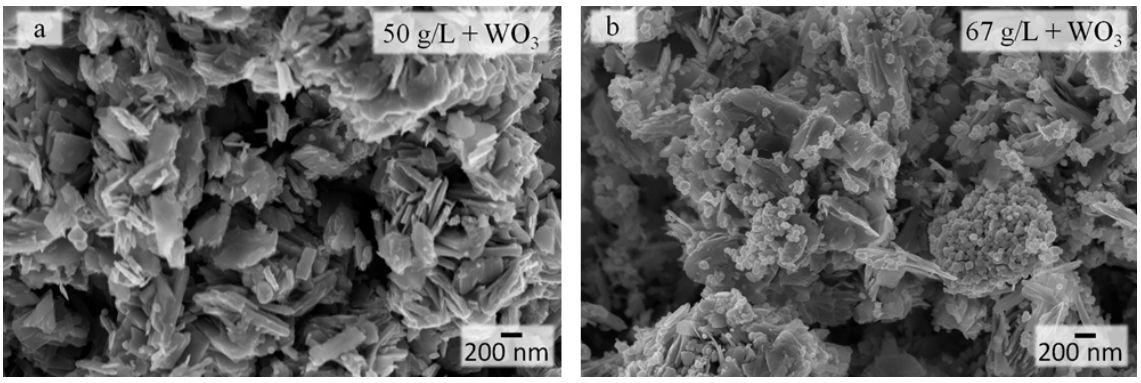

Figure 3.17: SEM images of the as-prepared combination of phases prepared using a) 50 g/L and b) 67 g/L of oxalic acid concentration samples.

3.3 Application of VO_x nanosheets as cathode

Two-dimensional nanostructured materials have been established to be potential electrodes for energy storage thanks to their enhanced electrochemical performance.

As reported in literature [10, 17] V_6O_{13} and VO_2 (B) nanosheets make an excellent candidate for cathode material in Li-ion batteries and this section describes the growth and layering nanosheets on FTO and ITO.

With a fixed molar ratio at 1:3 (V_2O_5:oxalic acid), 0.5 g of vanadium pentoxide (V) and 1 g of oxalic acid were dissolved in 20 mL and 15 mL of deionized water, respectively. Then, after thirty minutes of sonication at room temperature, VO_x was synthesized by hydrothermal synthesis assisted by microwave irradiation for twenty minutes with a temperature of 180 °C. Afterwards, the resultant black powder was washed by centrifugation with deionized water and ethanol for several times and dried by a vacuum process at 65 °C over night. The as-prepared powders were then annealed at 260 °C in a nitrogen atmosphere at 10 K/min.

The following SEM images (Fig.3.18) of the nanosheets revealed that the different concentrations impacts morphology, since the 50 g/L of oxalic acid concentration sample only presents nanosheets, while at 67 g/L of oxalic acid concentrations two structural morphologys appear, nanosheets and nanowires.

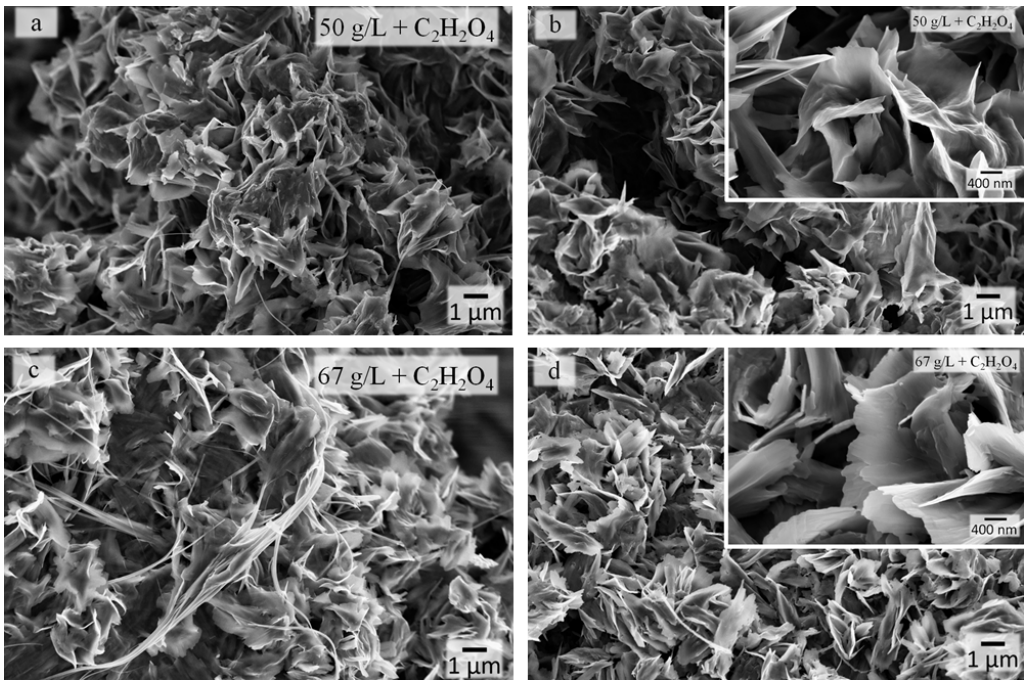

Figure 3.18: SEM images of the as-prepared VO_x nanosheets a) and c) before annealing, and b) and d) after annealing at 260 °C, with the inset of the annealed powders.

The as-prepared powders were then studied by XRD analysis, a summary of the phases is shown in Table 3.5. First, due to the XRD patterns similarities the observed peaks can infer that the different powders have the same phase.

Table 3.5: Phases and annealing temperatures of the as-pepared powders, respectively.

	Temperature (°C)	
Oxalic acid concentration (g/L)	Before annealing	After annealing (260)
50	VO_2 (B) or V_6O_{13}	VO_2 (B) or V_6O_{13}
67	VO_2 (B) or V_6O_{13}	VO_2 (B) or V_6O_{13}

The as-prepared powders (50 g/L and 67 g/L of oxalic acid concentration), shows peaks that may be correlated to VO_2 (B) (ICSD #01-081-2392), with the main indexed peaks (200), (110) and (-401) or to monoclinic V_6O_{13} (ICSD #01-075-1140) with the planes (110), (200) and (-401). To note that peaks correlated with (00l) planes are not observed in the diffractions patterns, which may be related with the nanosheets morphology (two dimensional) that leads to a planar growth (h00, 0k0) and not a columnar (00l). Since the observed orientation planes are the same for all samples it is not possible to attribute a specific VO_x phase with certainty.

For the annealed powders, the 50 g/L concentration has the same similarities as the before annealed powders, the relative intensity of the peaks varies to a lower intensity. Whereas for the annealed 67 g/L concentration the same lower intensity is observed,

together with a new peak at 23.1° and the extinction of the 15.8° peak. However, the difficulty remains and a VO_x phase was not correlated, the new peak was not indexed too.

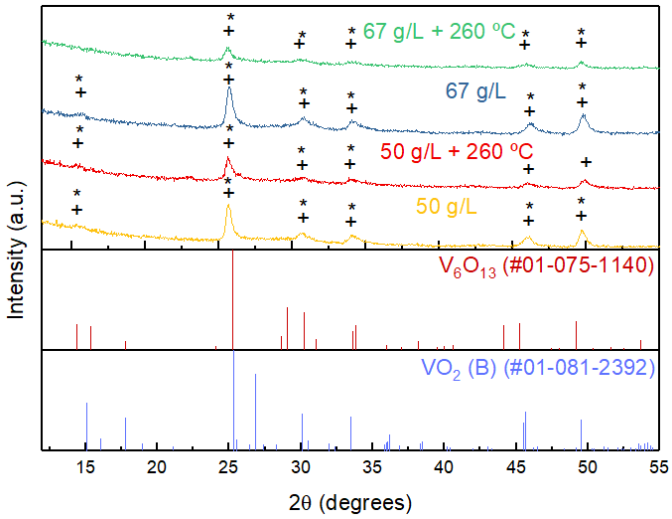

Figure 3.19: XRD diffractograms of the resultant powders prepared using 50 and 67 g/L of oxalic acid concentration before and after annealing.

A DSC thermogram of the annealed as-prepared powders was carried out. By observing Fig. 3.20 a very broad endothermic peak at 118.9 °C and 119 °C, corresponding to the 67 g/L and 50 g/L of oxalic acid concentration respectively, is perceived.

Since the very broad peaks are similar and in the same range as the already observed peaks in the remaining DSC thermogram regarding oxalic acid (Fig. 3.13 b) these very broad peak may be correlated to an electrochemical behaviour associated with VO_2 (B) and V_6O_{13}.

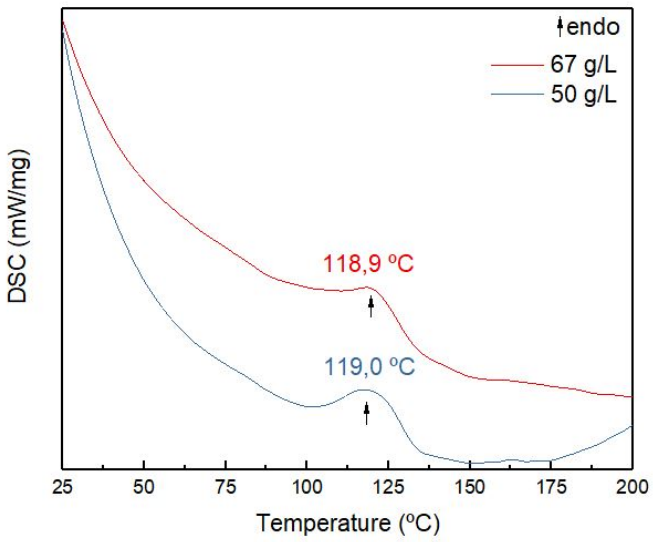

Figure 3.20: DSC thermogram of the as-prepared annealed powders of the samples prepared using 50 g/L and 67 g/L of oxalic acid concentrations.

3.3.1 VO_x nanosheets growth on ITO and FTO

During the hydrothermal synthesis of vanadium oxides phases, nanosheets with excellent electrochemical properties were achieved.

Using identical conditions as the above mentioned procedure several samples were prepared. First, ITO and FTO coated glass were cut in squares of 2x2 cm, washed with isopropyl alcohol in ultrasounds for ten minutes and then exposed to the UV light for fifteen minutes.

As growth mechanism several seed layers were coated by spin coating or PVD, where two groups were formed. The first group was coated with three layers of the prepared solution by spin coating (3000 rpm, 35 s) where each layer was annealed for four minutes on a hot plate at 100 °C.

The second group had a predeposition of amorphous VO_2 by e-beam assisted thermal evaporation, with a pressure deposition between 4 μPa and 5 $1mu$Pa, the melting pot had a current between 15 and 25 mA and a deposition rate of 0.5 and 3 Å/s. The thickness was controlled by a piezoelectric crystal combined with a thickness measurer. A third group was created where the samples were on the same conditions as described, but without seed layers (Fig. 3.21).

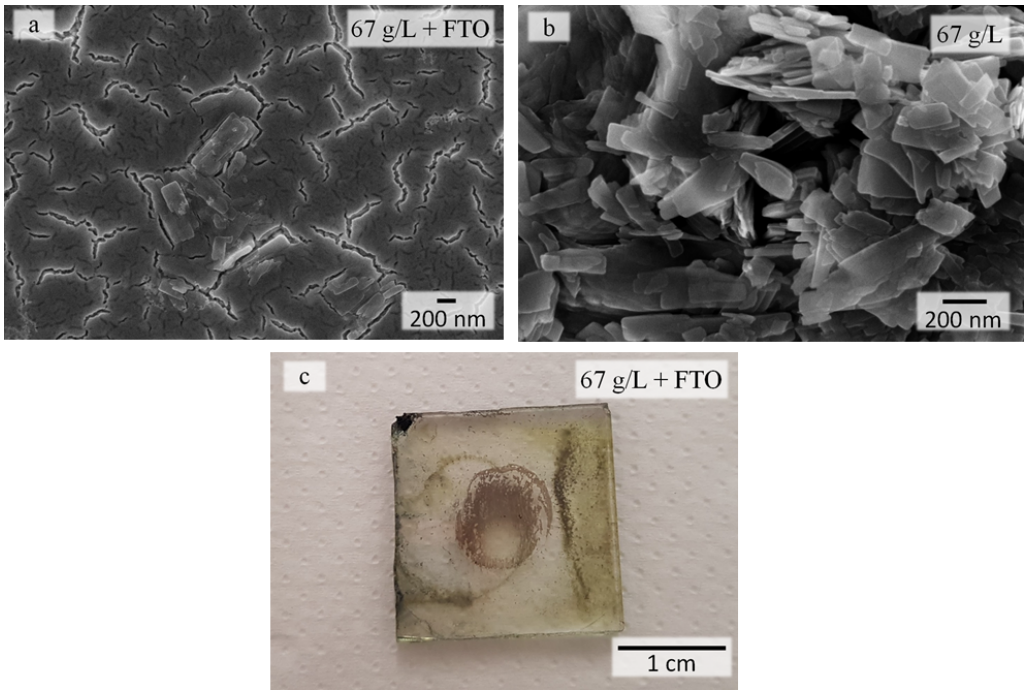

Figure 3.21: SEM images of a) FTO coated glass with nanosheets , b) as-prepared nanosheets prepared using 67 g/L of oxalic acid concentration and c) a photo of the FTO (2x2 cm) after the hydrothermal synthesis.

All groups, after deposition, were placed under microwave irradiation. However, after this process, no samples showed the coated seed layers or adhesion of nanoparticles. After changing the hydrothermal synthesis parameters, namely temperature, pressure and time

several times, it was concluded that the temperature, prior at 180 °C, was too high, preventing an adhesion of the nanoparticles. During the experiments, an adequate temperature of 160 °C was reached with the nanosheets remaining with good morphological structure.

At this temperature the only sample presenting a few nanosheets was the FTO coated glass with 67 g/L of oxalic acid concentration, as shown in Fig 3.21.

3.3.2 VO_x nanosheets deposition on ITO and FTO

In this section, as-prepared powders were layered in order to create a homogeneous film of nanosheets.

Two different deposition techniques types were evaluated, the first was deposition by spin coating of the as-prepared nanosheets powder dispersed in ethanol (3000 rpm, 20 s) followed by an annealing for each layer at 100 °°, however, this deposition was not successful, the film was not homogeneous and the particles tended to aggregate.

Secondly, a deposition by airbrush pen system, where the as-prepared powders, Fig. 3.22 a), were dispersed in a solution of ethanol, with a concentration of 4.5 g/L, and sonicated for forty five minutes. Also, ITO and FTO coated glass were cleaned and UV exposed as explained in section 3.3.1.

ITO and FTO coated glasses were placed on a hot plate at 120 °C and left for three minutes. Then the prepared suspension was sequentially sprayed onto the substrates, allowing to the ethanol evaporate between sprays. After the ITO and FTO samples are completely and uniformly covered with the nanosheets, they were left to cool at room temperature. The nanosheets coverage was uniform and as Fig. 3.22 b) shows.

In order to observe if the prepared sample could be applied as cathode, it was tested in an electrochemical cell in a beaker with 30 mL of electrolyte $LiClO_4$. Here a metal wire which acts as the counter electrode and the sample, which is the working electrode, were connected to a voltage source and submerged in the electrolyte as shown in Fig. 3.22 c).

A 3 V potential between the working electrode and the counter electrode was applied resulting in a maximum current of 1.46 mA and 1.75 mA in FTO and ITO, respectively. During the experiment the current decreased in both samples due to the degradation of the layered nanosheets. The same test was performed with ITO and FTO without VO_x nanosheets and the maximum current was 0.13 mA for FTO and 0.11 mA for ITO.

The color of the powder remained the same, except for a light discoloration from the degradation, proving that the as-prepared powders do not have an eletrochromic behaviour, but a good electrochemical performance.

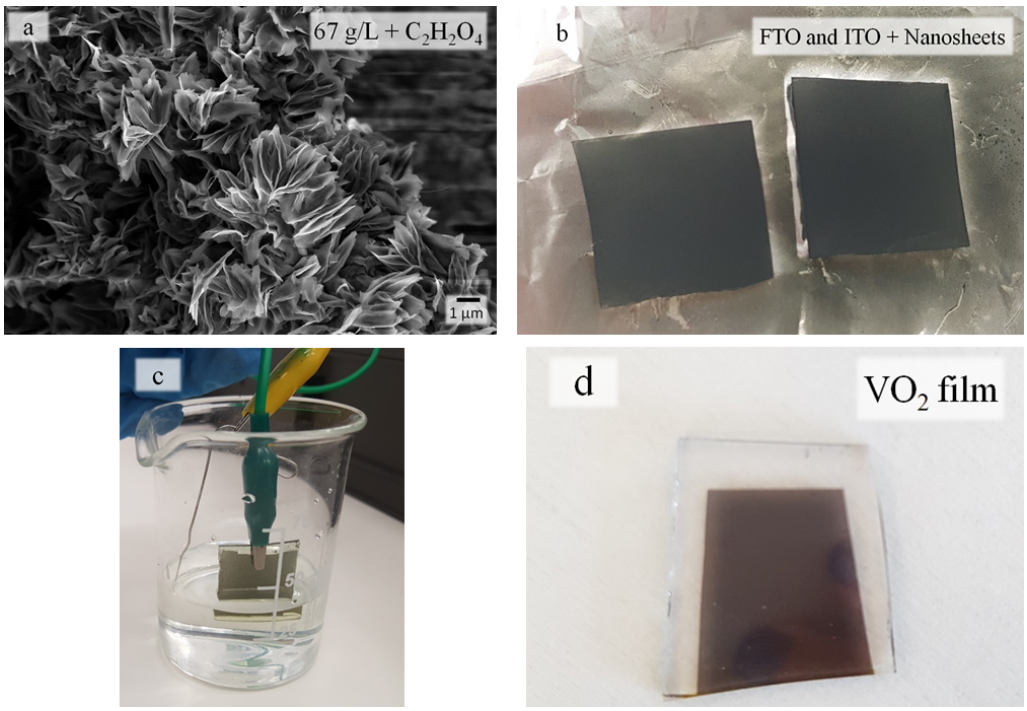

Figure 3.22: a) SEM image of the as-prepared powder, b) ITO and FTO samples with the deposited as-prepared VO_x nanosheets powder, c) the experiment with the electrolyte and ITO + nanosheets and d) FTO with a pre-deposition of amorphous VO_2.

4

Conclusion and future perspectives

In this work, the synthesis of vanadium oxides through microwave irradiation were investigated and achieved. The influence of synthesis parameters were studied and several phases were accomplish. The study was sustained by morphological and crystalline structure analysis by SEM, TG-DSC, UV-vis-NIR reflectance spectroscopy and X-Ray Diffraction, respectively.

The results of the precursor influence showed that VO_2 (B), V_3O_7, V_6O_{13} and V_2O_5 phases can be obtained, as single phase or phase combination, with both reducing agents (citric acid and oxalic acid), however, the thermochromic phase vanadium dioxide (VO_2 (M2) was only achieved with the reducing agent citric acid, meaning that the phase transformation is indeed influenced by the reducing agent.

Furthermore, the morphology is also influenced by which reducing agent is used, since oxalic acid allows the basic structures nanosheets, nanowires and nanoplatelets, while citric acid only permit nanoplatelets and spherical shape nanostructures. Also, depending on the concentration the dissolution method may, or may not have an influence as observed with the precursor oxalic acid. In addition, the same can be concluded for the washing process for both reducing agents.

Different concentrations of reducing agent have indeed implications in morphology, since at higher concentrations (57 and 67 g/L) the predominant nanostructure are nanosheets, whereas, at lower concentrations (18, 35 and 35 g/L) the dominant structure are nanoplatelets.

The analysis about concentration and ratios are extremely important, since the reduction only succeeds in a small range of concentration values such as 18, 25, 35, 50 and 67 g/L for oxalic acid, while for citric acid is 26 and 50 g/L.

At different annealing temperatures, the lower concentrations may lead to VO_2 (B) and V_2O_5 for both reducing agents and for higher concentrations may lead to V_6O_{13} and V_3O_7 phases, implicating that different concentrations originates different structural arrangements. Nevertheless, a combination of VO_x phase was accomplished leading to believe that a higher nitrogen pressure is needed.

An interesting point to emphasize is that the orientation planes (00l) were not observed in the VO_x nanosheets diffraction patterns, this might happen due to the morphology which is mainly a two dimensional structure, meaning that the growth is only planar and not columnar.

In addition, several DSC thermogram were carried out and in all analysis very broad peaks. These values are not reported in literature and are present in all samples, leading to the belief that is an intrinsic property of the as-prepared VO_x phases powders.

Hydrothermal synthesis temperature was also considered a critical factor in both reducing agents, which is determining to obtained a resultant powder, in a range of 160 °C to 180 °C pure phases were formed. A temperature of 180 °C lead to the best crystalline structure among the samples.

During the experiments a VO_x nanosheets structure was reached with the following synthesis parameters, 50 g/L and 67 g/L of oxalic acid concentration, with a 1:3 (V_2O_5:oxalic acid) molar ratio, sonication for thirty minutes, a synthesis temperature of 180 °C for twenty minutes, pressure of 250 Psi, a power of 250 W and a washing process with ethanol and deionized water. Due to the good morphological structure of the samples it was successfully applied as cathode in an electrochemical cell. The current obtained when using VO_x covered ITO and FTO was 10 times higher than for the pristine ITO and FTO. In order to further evaluate the electrochemical performance of the nanosheets cyclic voltammetry should be performed.

In spite of these achievements, further studies are required. The investigation of other parameters, such as pH, vanadium oxide concentration, a different reducing agent and their impact in the morphological structure, while other parameters are kept constant and an attempt to reach a pure VO_x phase by hydrothermal synthesis assisted by microwave irradiation.

Also, an attempt to optimize nanosheets as application as cathode and try different deposition processes in the same substrates, should also be a future study.

Bibliography

[1] R. Minch, K. R. Moonoosawmy, C. H. Solterbeck, and M. Es-Souni. "The influence of processing conditions on the morphology and thermochromic properties of vanadium oxide films." In: *Thin Solid Films* 556 (2014), pp. 277–284.

[2] G. K. Dalapati, A. K. Kushwaha, M. Sharma, V. Suresh, S. Shannigrahi, S. Zhuk, and S. Masudy-Panah. "Transparent heat regulating (THR) materials and coatings for energy saving window applications: Impact of materials design, micro-structural, and interface quality on the THR performance." In: *Progress in Materials Science* 95 (2018), pp. 42–131.

[5] S. Xu, D. Cen, P. Gao, H. Tang, and Z. Bao. "3D Interconnected V6O13Nanosheets Grown on Carbonized Textile via a Seed-Assisted Hydrothermal Process as High-Performance Flexible Cathodes for Lithium-Ion Batteries." In: *Nanoscale Research Letters* 13 (2018), pp. 1–7.

[6] S. Hoffmann, E. S. Lee, and C. Clavero. "Examination of the technical potential of near-infrared switching thermochromic windows for commercial building applications." In: *Solar Energy Materials and Solar Cells* 123 (2014), pp. 65–80.

[7] H. Ji, D. Liu, H. Cheng, C. Zhang, L. Yang, and D. Ren. "Infrared thermochromic properties of monoclinic VO2nanopowders using a malic acid-assisted hydrothermal method for adaptive camouflage." In: *RSC Advances* 7.9 (2017), pp. 5189–5194.

[8] A. A. Akande, E. C. Linganiso, B. P. Dhonge, K. E. Rammutla, A. Machatine, L. Prinsloo, H. Kunert, and B. W. Mwakikunga. "Phase evolution of vanadium oxides obtained through temperature programmed calcinations of ammonium vanadate in hydrogen atmosphere and their humidity sensing properties." In: *Materials Chemistry and Physics* 151 (2015), pp. 206–214.

[9] N. Bahlawane and D. Lenoble. "Vanadium oxide compounds: Structure, properties, and growth from the gas phase." In: *Chemical Vapor Deposition* 20.7-9 (2014), pp. 299–311.

[10] Z. Zou, H. Cheng, J. He, F. Long, Y. Wu, Z. Yan, and H. Chen. "V6O13nanosheets synthesized from ethanol-aqueous solutions as high energy cathode material for lithium-ion batteries." In: *Electrochimica Acta* 135 (2014), pp. 175–180.

[11] N. Peys, Y. Ling, D. Dewulf, S. Gielis, C. De Dobbelaere, D. Cuypers, P. Adriaensens, S. Van Doorslaer, S. De Gendt, A. Hardy, and M. K. Van Bael. "V6O13 films by control of the oxidation state from aqueous precursor to crystalline phase." In: *Dalton Transactions* 42.4 (2013), pp. 959–968.

[12] Y. Zhang. "VO2(B) conversion to VO2(A) and VO2(M) and their oxidation resistance and optical switching properties." In: *Materials Science- Poland* 34.1 (2016), pp. 169–176.

[13] D. Alie, L. Gedvilas, Z. Wang, R. Tenent, C. Engtrakul, Y. Yan, S. E. Shaheen, A. C. Dillon, and C. Ban. "Direct synthesis of thermochromic VO2through hydrothermal reaction." In: *Journal of Solid State Chemistry* 212 (2014), pp. 237–241.

[14] P. Kiria, G. Hyett, and R. Binionsa. "Solid state thermochromic materials." In: *Advanced Materials Letters* 1.2 (2010), pp. 86–105.

[15] R. Enjalbert and J. Galy. "A refinement of the structure of V2O5." In: *Acta Crystallographica Section C Crystal Structure Communications* 42.11 (1986), pp. 1467–1469.

[16] G. R. Mutta, S. R. Popuri, P. Ruterana, and J. Buckman. "Single step hydrothermal synthesis of mixed valent V6O13nano-architectures: A case study of the possible applications in electrochemical energy conversion." In: *Journal of Alloys and Compounds* 706 (2017), pp. 562–567.

[17] Q. Wang, J. Pan, M. Li, Y. Luo, H. Wu, L. Zhong, and G. Li. "VO2 (B) Nanosheets as a Cathode Material for Li-ion Battery." In: *Journal of Materials Science and Technology* 31.6 (2015), pp. 630–633.

[18] M. S. Pawar, M. A. Sutar, K. I. Maddani, and S. G. Kandalkar. "Improvement in Electrochemical Performance of Spray Deposited V2O5Thin Film Electrode by Anodization." In: *Materials Today: Proceedings* 4.2 (2017), pp. 3549–3556.

[3] H. Wang, M. Barrett, B. Duane, J. Gu, and F. Zenhausern. "Materials and processing of polymer-based electrochromic devices." In: *Materials Science and Engineering B: Solid-State Materials for Advanced Technology* 228.July 2017 (2018), pp. 167–174.

[19] C. G. Granqvist, M. A. Arvizu, I. Bayrak Pehlivan, H. Y. Qu, R. T. Wen, and G. A. Niklasson. "Electrochromic materials and devices for energy efficiency and human comfort in buildings: A critical review." In: *Electrochimica Acta* 259 (2017), pp. 1170–1182.

[20] B. P. Jelle. "Solar radiation glazing factors for window panes, glass structures and electrochromic windows in buildings - Measurement and calculation." In: *Solar Energy Materials and Solar Cells* 116.7465 (2013), pp. 291–323.

[4] A. Gonçalves, J. Resende, A. C. Marques, J. V. Pinto, D. Nunes, A. Marie, R. Goncalves, L. Pereira, R. Martins, and E. Fortunato. "Smart optically active VO2nanostructured layers applied in roof-type ceramic tiles for energy efficiency." In: *Solar Energy Materials and Solar Cells* 150 (2016), pp. 1–9.

[21] S. Zhang, B. Shang, J. Yang, W. Yan, S. Wei, and Y. Xie. "From VO2(B) to VO2(A) nanobelts: First hydrothermal transformation, spectroscopic study and first principles calculation." In: *Physical Chemistry Chemical Physics* 13.35 (2011), pp. 15873–15881.

[22] T. V. O. M, S. R. Popuri, M. Miclau, A. Artemenko, C. Labrugere, and A. Villesuzanne. "Rapid Hydrothermal Synthesis of VO 2 (B) and Its Conversion to." In: *Inorganic chemistry* 2 (2013), pp. 4780–4785.

[23] X. Li, L. Yang, S. Zhang, X. Li, J. Chen, and C. Huang. "VO2(M) with narrow hysteresis width from a new metastable phase of crystallized VO2(M) · 0.25H2O." In: *Materials Letters* 211 (2018), pp. 308–311.

[24] P. Liu, K. Zhu, Y. Gao, Q. Wu, J. Liu, J. Qiu, Q. Gu, and H. Zheng. "Ultra-long VO2 (A) nanorods using the high-temperature mixing method under hydrothermal conditions: synthesis, evolution and thermochromic properties." In: *CrystEngComm* 15.14 (2013), p. 2753.

[25] D. Hagrman, J. Zubieta, C. J. Warren, L. M. Meyer, M. M. J. Treacy, and R. C. Haushalter. "A New Polymorph of VO2Prepared by Soft Chemical Methods." In: *Journal of Solid State Chemistry* 138.1 (1998), pp. 178–182.

[26] Y. Gao, H. Luo, Z. Zhang, L. Kang, Z. Chen, J. Du, M. Kanehira, and C. Cao. "Nanoceramic VO2thermochromic smart glass: A review on progress in solution processing." In: *Nano Energy* 1.2 (2012), pp. 221–246.

[27] W. Li, S. Ji, Y. Li, A. Huang, H. Luo, and P. Jin. "Synthesis of VO2 nanoparticles by a hydrothermal-assisted homogeneous precipitation approach for thermochromic applications." In: *RSC Advances* 4.25 (2014), pp. 13026–13033.

[28] W. Li, S. Ji, K. Qian, and P. Jin. "Preparation and characterization of VO2 (M)-SnO2 thermochromic films for application as energy-saving smart coatings." In: *Journal of Colloid and Interface Science* 456 (2015), pp. 166–173.

[29] S. Wang, M. Liu, L. Kong, Y. Long, X. Jiang, and A. Yu. "Recent progress in VO2smart coatings: Strategies to improve the thermochromic properties." In: *Progress in Materials Science* 81 (2016), pp. 1–54.

[30] S. C. Barron, J. M. Gorham, M. P. Patel, and M. L. Green. "High-throughput measurements of thermochromic behavior in V(1- x)Nb(x)O2 combinatorial thin film libraries." In: *ACS Combinatorial Science* 16.10 (2014), pp. 526–534.

[31] H. K. Chen, H. C. Hung, T. C. K. Yang, and S. F. Wang. "The preparation and characterization of transparent nano-sized thermochromic VO2-SiO2films from the sol-gel process." In: *Journal of Non-Crystalline Solids* 347.1-3 (2004), pp. 138–143.

[32] S. Chen, L. Dai, J. Liu, Y. Gao, X. Liu, Z. Chen, J. Zhou, C. Cao, P. Han, H. Luo, and M. Kanahira. "The visible transmittance and solar modulation ability of VO2flexible foils simultaneously improved by Ti doping: An optimization and first principle study." In: *Physical Chemistry Chemical Physics* 15.40 (2013), pp. 17537–17543.

[33] G. A. Niklasson, S.-Y. Li, and C. G. Granqvist. "Thermochromic vanadium oxide thin films: Electronic and optical properties." In: *Journal of Physics: Conference Series* 559.November (2014), p. 012001.

[34] D. Vernardou, D. Louloudakis, E. Spanakis, N. Katsarakis, and E. Koudoumas. "Thermochromic amorphous VO2coatings grown by APCVD using a single-precursor." In: *Solar Energy Materials and Solar Cells* 128 (2014), pp. 36–40.

[35] M. M. Seyfouri and R. Binions. "Sol-gel approaches to thermochromic vanadium dioxide coating for smart glazing application." In: *Solar Energy Materials and Solar Cells* 159 (2017), pp. 52–65.

[36] D. P. Partlow, S. R. Gurkovich, K. C. Radford, and L. J. Denes. "Switchable vanadium oxide films by a sol-gel process." In: *Journal of Applied Physics* 70.1 (1991), pp. 443–452.

[37] S. Ji, Y. Zhao, F. Zhang, and P. Jin. "Direct formation of single crystal VO2(R) nanorods by one-step hydrothermal treatment." In: *Journal of Crystal Growth* 312.2 (2010), pp. 282–286.

[38] H. Fei, Y. Lin, and M. Wei. "Facile synthesis of V6O13micro-flowers for Li-ion and Na-ion battery cathodes with good cycling performance." In: *Journal of Colloid and Interface Science* 425 (2014), pp. 1–4.

[39] F. Cheng, J. Liang, Z. Tao, and J. Chen. "Functional materials for rechargeable batteries." In: *Advanced Materials* 23.15 (2011), pp. 1695–1715.

[40] T. Toriyama, T. Nakayama, T. Konishi, and Y. Ohta. "Charge and orbital orderings associated with metal-insulator transition in V6 O13." In: *Physical Review B - Condensed Matter and Materials Physics* 90.8 (2014), pp. 1–9.

[41] P. D. Dernier. "Structural investigation of the metal-insulator transition in V6O13." In: *Materials Research Bulletin* 9.7 (1974), pp. 955–963.

[42] Z. Huang, H. Zeng, L. Xue, X. Zhou, Y. Zhao, and Q. Lai. "Synthesis of vanadium oxide, V6O13hollow-flowers materials and their application in electrochemical supercapacitors." In: *Journal of Alloys and Compounds* 509.41 (2011), pp. 10080–10085.

[43] Y. Zhang and C. Meng. "Facile one-pot hydrothermal synthesis of belt-like β-V6O13 with rectangular cross sections for Li-ion battery application." In: *Materials Letters* 160 (2015), pp. 404–407.

[44] Y. Zhu, Z. Huang, Z. Hu, L. Xi, X. Ji, and Y. Liu. "3D interconnected ultrathin cobalt selenide nanosheets as cathode materials for hybrid supercapacitors." In: *Electrochimica Acta* 269 (2018), pp. 30–37.

[45] M. Sahana and S. Shivashankar. "Metalorganic chemical vapor deposition of highly oriented thin film composites of V2O5 and V6O13: Suppression of the metal–semiconductor transition in V6O13." In: *Journal of Materials Research* 19.10 (2004), pp. 2859–2870.

[46] A. Rúa, F. E. Fernández, R. Cabrera, and N. Sepúlveda. "Young's modulus of pulsed-laser deposited V6O13 thin films." In: *Journal of Applied Physics* 105.11 (2009), pp. 1–5.

[47] S. R. Bansode and V. K. Rathod. “Enzymatic sythesis of Isoamyl butyrate under microwave irradiation.” In: *Chemical Engineering and Processing - Process Intensification* 129.March (2018), pp. 71–76.

[48] G. R. Mutta, S. R. Popuri, M. Vasundhara, M. Maciejczyk, A. V. Racu, R. Banica, N. Robertson, J. I. Wilson, and N. S. Bennett. “Facile hydrothermal synthesis of economically viable VO2(M1) counter electrode for dye sensitized solar cells.” In: *Materials Research Bulletin* 83 (2016), pp. 135–140.

[49] H. Zhang. “Ultrathin Two-Dimensional Nanomaterials.” In: *ACS Nano* 9.10 (2015), pp. 9451–9469.

[50] A. C. Figueiredo. “Growth of Vanadium Dioxide (VO2) Nanostructures by Controlling the Hydrothermal Synthesis Parameters.” In: (2016).